A Binary Packing Material–Based Procedure for Evaluating Soil Liquefaction Triggering during Earthquakes

Guoxing Chen[1]; Qi Wu[2]; Kai Zhao[3]; Zhifu Shen[4]; and Jun Yang, F.ASCE[5]

Abstract: This paper presents a new approach to assess the liquefaction triggering of saturated sandy soils based on comprehensive laboratory datasets in conjunction with the concept of binary packing material for sandy soils. The equivalent skeleton void ratio (e^*_{sk}) is used as an alternative state index for sandy soils with fines content (FC) less than a threshold value (FC_{th}). To characterize the liquefaction triggering curve for the correlation between the cyclic resistance ratio (CRR_{15}) in 15 cycles and the corrected shear-wave velocity (V_{s1}), a series of undrained cyclic triaxial tests as well as bender element tests have been performed on six types of saturated sandy soils. A remarkable finding of the laboratory investigation is that both CRR_{15} and V_{s1} are virtually uniquely related with e^*_{sk} for all six sandy soils. This finding is confirmed by the experimental data on CRR_{15} and on V_{s1} for different sandy soils published in the literature. The parameters defining the relationships between CRR_{15} and e^*_{sk} between V_{s1} and e^*_{sk} can be simply determined through a unique set of explicit expressions which incorporate some basic index properties of the host sand and fines. In this regard, the proposed procedure provides a significant advantage in the evaluation of liquefaction triggering of sandy soils in practice. **DOI: 10.1061/(ASCE)GT.1943-5606.0002263.** © *2020 American Society of Civil Engineers.*

Author keywords: Soil liquefaction; Earthquakes; Cyclic loads; Binary packing materials; Equivalent skeleton void ratio.

Introduction

Soil liquefaction is known as one of the major causes of significant damage during earthquakes and is also a complicated phenomenon of long-standing interest in soil mechanics. Assessment of soil liquefaction potential has attracted considerable attention from engineers and researchers during the last five decades. Three of the most common in situ test methods, i.e., standard penetration testing (SPT), cone penetration testing (CPT), and shear-wave velocity (V_s) testing, have been extensively used to assess the liquefaction potential of saturated sandy and gravely soils in engineering practice. Evaluations of soil liquefaction potential are often conducted using liquefaction triggering charts calibrated by field case histories of liquefaction and/or nonliquefaction (e.g., Seed and Idriss 1971; Seed et al. 1985; Andrus and Stokoe 2000; Youd et al. 2001; Cetin et al. 2004, 2018; Idriss and Boulanger 2010; Boulanger and Idriss 2012; Kayen et al. 2013; Chen et al. 2015, 2017; among many others). Inherent to this procedure is that the seismic demand imposed on the soil at a given depth is defined as the earthquake-induced cyclic stress ratio (CSR), and the soil resistance to liquefaction in the field is defined as the cyclic resistance ratio (CRR), with liquefaction predicted if CSR > CRR. The empirical method makes use of field observations to develop relationships between the measured in situ parameters and CRR and adopt the simplified stress-based approach for calculating CSR.

The many available correlations relating the CRR of soil to in situ tests are subjected to a set of standard reference conditions: an initial vertical effective stress of 1 atm, earthquake moment magnitude $M_w = 7.5$, clean sand, and a level ground (sloping less than 6%). For situations that do not satisfy these standard reference conditions, adjustments to the measured in situ resistance parameters and CRR are required. The CRR correlations from SPT blow count proposed by Youd et al. (2001), Cetin et al. (2004), and Idriss and Boulanger (2010) are commonly used in practice. Chen et al. (2015) suggested a new CRR correlation based on the expanded SPT-based database of Idriss and Boulanger (2010) and Xie (1984). Cetin et al. (2018) presented an updated version of Cetin et al. (2004). The CRR correlations from the CPT data proposed by Robertson and Wride (1998), Moss et al. (2006), and Robertson (2009) are also used in practice, and the correlation by Robertson and Wride (1998) was recommended by the 1998 National Center for Earthquake Engineering Research (NCEER) Workshop (Youd et al. 2001). Ku et al. (2012) presented a probabilistic method for assessment of liquefaction potential using the database of Robertson (2009). The commonly used CRR correlations from V_s data are those developed by Andrus and Stokoe (2000) and Kayen et al. (2013). Using an expanded global database of case histories, Chen et al. (2017) developed a new calibrated CRR-V_s correlation for liquefaction triggering analysis. Each empirical method calibrated from field case histories has merits and disadvantages and has a certain amount of uncertainty. The uncertainty is associated with, for example, measured field data, site-specific ground motions, and the adjustment factors applied to evaluate the CRR. It is thus important to identify and characterize soil type and the detailed variations in the in situ resistance within a soil profile for assessment of the liquefaction susceptibility. However, the SPT method has a limitation to identify thinner layers or detailed variations within

[1]Professor, Institute of Geotechnical Engineering, Nanjing Tech Univ., Nanjing 210009, China; Director, Civil Engineering and Earthquake Disaster Prevention Center of Jiangsu Province, Nanjing 210009, China (corresponding author). Email: gxc6307@163.com

[2]Ph.D. Student, Institute of Geotechnical Engineering, Nanjing Tech Univ., Nanjing 210009, China.

[3]Associate Professor, Institute of Geotechnical Engineering, Nanjing Tech Univ., Nanjing 210009, China.

[4]Associate Professor, Institute of Geotechnical Engineering, Nanjing Tech Univ., Nanjing 210009, China.

[5]Professor, Dept. of Civil Engineering, Univ. of Hong Kong, Hong Kong, China.

Note. This manuscript was submitted on April 6, 2019; approved on January 14, 2020; published online on March 28, 2020. Discussion period open until August 28, 2020; separate discussions must be submitted for individual papers. This paper is part of the ***Journal of Geotechnical and Geoenvironmental Engineering***, © ASCE, ISSN 1090-0241.

a soil profile, while the CPT and V_s loggings cannot provide a direct measurement of soil type due to lack of soil sampling. Furthermore, the applicability of the field-based methods to assess the liquefaction triggering potential of soils with significant fines content (FC) (i.e., percent smaller than 0.075 mm) remains unclear. Several studies have pointed out the limitations of these SPT, CPT, and V_s triggering charts (e.g., Youd et al. 2001; Dobry et al. 2015).

Based on a combination of postearthquake observational field data and index property tests (e.g., Atterberg limits, grain size and distribution, density), several screening criteria for assessing liquefaction susceptibility of a soil containing fines have been proposed (e.g., Seed et al. 2003; Bray and Sancio 2006; Boulanger and Idriss 2006). Because the granular soils with significant fines generally are amenable to undisturbed sampling, the screening criteria involving laboratory measurements of Atterberg limits (e.g., liquid limit and plasticity index) and water content may yield conflicting conclusions in some situations. Cyclic laboratory tests (cyclic triaxial, direct simple shear, and hollow cylinder torsional shear) are often used to assist the liquefaction evaluation and provide insight into the deformation and excess pore-water pressure generation (Silver and Seed 1971; Martin et al. 1975; Dobry et al. 1982; Tokimatsu et al. 1986; Green and Terri 2005; Yang and Sze 2011a, b; Chen et al. 2019, 2020). The effect of the scenario earthquake in the cyclic laboratory tests to a liquefaction- susceptible soil is characterized by CSR and number of uniform loading cycles (N) as a function of M_w, cyclic loading pattern, and stress path. Conflicting trends have been reported in the literature that the CRR of sandy soils is increasing, decreasing, or unaffected with increasing FC (e.g., Lade and Yamamuro 1997; Amini and Qi 2000; Polito and Martin 2001). The reason for these seemingly contradictory trends can be explained qualitatively using relative density (D_r) or global void ratio (e) of silt-sand mixtures (sandy soils) as the basic index properties, and there is a concern that what is an appropriate state variable for characterizing the behavior of the sandy soils below limiting FC (Yang et al. 2015). In addition, for cyclic laboratory tests, the residual excess pore-water pressure (u_e) is usually expressed as an excess pore-water pressure ratio (r_u), defined as the ratio of the u_e to the initial effective consolidation stress (σ'_{c0}) acting on the soil during the undrained cyclic testing, and CRR is generally defined as the applied CSR that causes initial liquefaction (r_u of 100%) or a certain widely accepted strain level (e.g., double-amplitude axial strain $\varepsilon_{da} = 5\%$) after a certain number of uniform loading cycles. The cyclic strength curve, used to characterize the liquefaction resistance of a soil, is related to the specific value of the CRR to use in assessing liquefaction potential based on the equivalent number of uniform cycles of loading (N_{eq}), which represents the number of uniform cycles for the scenario earthquake. Thus, the determination of N_{eq} value is an important issue in cyclic laboratory testing for assessing liquefaction triggering, but there is no consensus on N_{eq} value for use in the evaluation of liquefaction triggering. The assumption that the equivalency of stress cycles is the same as the equivalency of strain cycles is uncertain (Green and Terri 2005; NASEM 2016).

Tokimatsu et al. (1986) found that the same soil samples reconstituted by various methods to the same V_s have a similar CRR. Subsequently, several investigators reconstituted samples in the laboratory to the same V_s measured in situ (e.g., Wang et al. 2006; Baxter et al. 2008), exemplifying that the CRR of the reconstituted samples was similar to that of the undisturbed samples. The results of Ahmadi and Paydar (2014) showed that there is a good soil-specific relationship between laboratory measurements of V_s and CRR. It is thus desirable to establish a relationship between CRR and V_s for sandy soils to assess their liquefaction potential.

Table 1. Capacity, deviations, and precision of the cyclic triaxial testing apparatus in this study

Controller	Capacity	Deviation	Precision
Axial force	5 kN	0.1% FS	0.2 N
Axial displacement	±50 mm	0.15% FS	0.2 μm
Cell/back pressure	2 MPa	0.15% FS	1 kPa
Cell/back volume	200 mL	0.25% FS	1 mm^3
Pore pressure	2 MPa	0.15% FS	1 kPa

Note: FS = full-scale range.

The goal of the present study is to find a laboratory testing-based simple method for assessing CRR and V_s of liquefiable sandy soils. To this end, a series of stress-controlled undrained cyclic triaxial (CTX) tests as well as bender element (BE) tests have been conducted on six different sandy soils to explore the relationships between CRR and V_s with respect to various physical properties of the soils. Literature data on 12 types of sandy soils for assessing CRR and on eight types of sandy soils for assessing V_s have been compiled and analyzed. It is demonstrated that the new method, developed from this large database, has a significant advantage in practical applications.

Test Apparatus, Materials, and Methods

Testing Apparatus

CTX tests were performed using an automated triaxial apparatus which uses an internal submersible load cell to measure the axial force and a high-quality linear variable differential transformer to measure the axial displacement. Table 1 shows the capacity, measurement deviations, and precisions of the sensors under various physical conditions (Chen et al. 2016; Zhuang et al. 2018).

V_s measurements were independently performed using a pair of piezoceramic BEs installed in the top and bottom platens of the cell chamber of a dynamic hollow/solid cylinder apparatus (HCA) (Chen et al. 2019).

Tested Materials

Six clean sands, including Fujian sand (FJS), Fujian sand-I (FJS-I), Fujian sand-II (FJS-II), Nanjing sand (NJS), Nantong sand (NTS), and Yunnan sand (YNS), were used as host sands in the laboratory tests. Fujian sand is pure siliceous sand with round particle shapes and is defined as a kind of standard sand in China. Nanjing sand is a schistose, fine sand with dark color that is composed predominantly of siliceous grains, including chlorite, mica, clay, and clastic materials. Yunnan sand is subangular crushed granite sand, composed of approximately 42% quartz, 33% potassium feldspar, and 18% plagioclase, with less than 7% biotite and amphibole minerals. Nantong sand is a fine-grained, angular siliceous sand. Nantong silt with subangular particles was used as nonplastic silica fines (pure fines) to investigate the effects of FC on the liquefaction resistance of sandy soils. The six host sands were mixed with nonplastic Nantong silt (pure fines) corresponding to various FC from 0% to 30% by mass. With the ASTM test standards, the particle-size distributions (PSDs) of the six sandy soils with various FC and the pure fines used in the tests as well as the 14 sandy soils from the literature are presented in Fig. 1. The scanning electron microscopy images or digital camera diagrams of four host sands and pure fines are also shown in Fig. 1. The minimum and maximum void ratios ($e_{\min}$ and $e_{\max}$) of the tested six types of sandy soils with various nonplastic FC, determined according to ASTM test standards, are

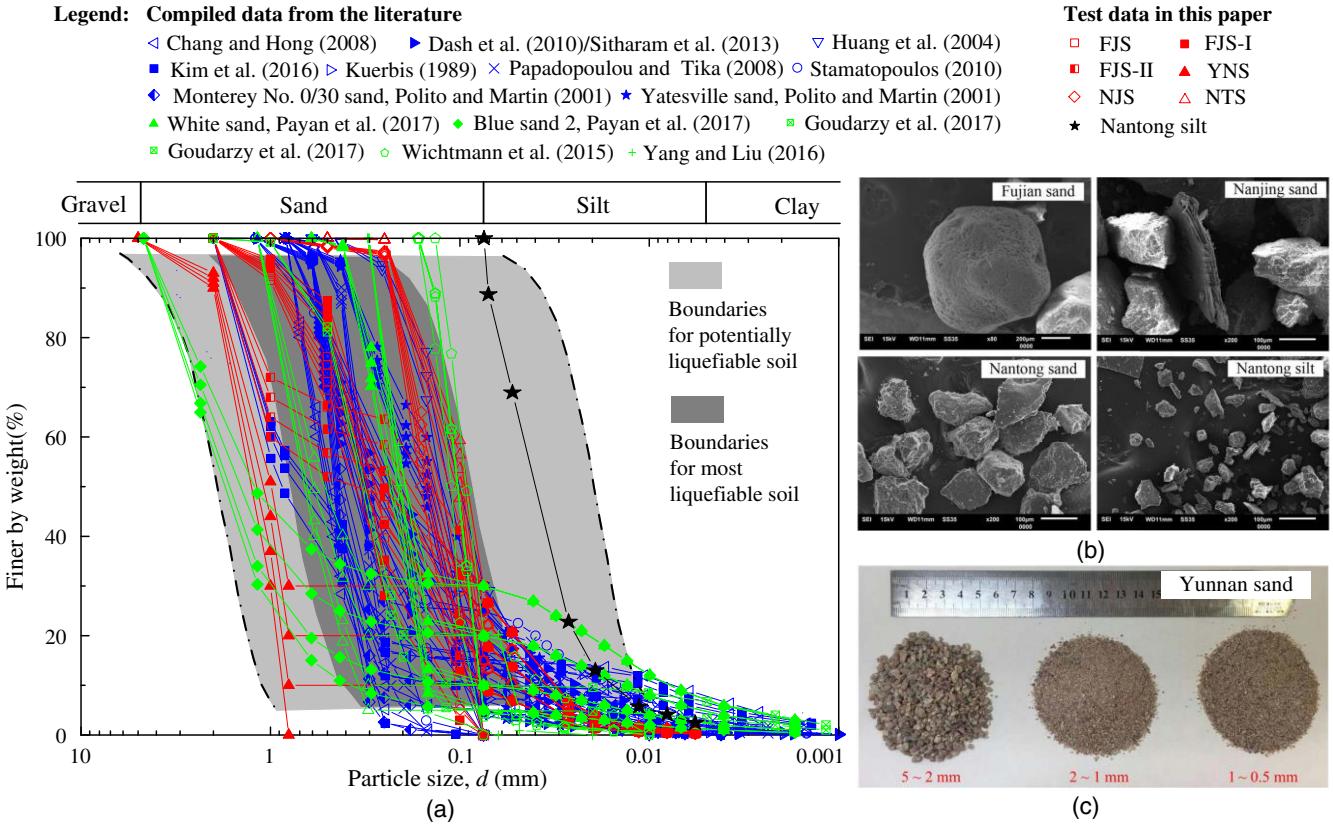

Fig. 1. (a) Particle size distributions of six sandy soils and silt in this paper and of 14 sandy soils using compiled data from the tests of Kuerbis (1989), Polito and Martin (2001), Huang et al. (2004), Chang and Hong (2008), Papadopoulou and Tika (2008), Dash et al. (2010), Stamatopoulos (2010), Sitharam et al. (2013), Wichtmann et al. (2015), Goudarzy et al. (2016), Kim et al. (2016), Yang and Liu (2016), and Payan et al. (2017); (b) optical microscope images of three host sands and Nantong silt (pure fines) in this paper; and (c) digital camera photos of Yunnan sand in this paper.

presented in Fig. 2. Table 2 gives the index properties of the host sands and pure fines for 20 types of sandy soils tested in this study and collected from the literature. Therefore, the mineral composition and particle-size distribution of Yunnan sand (host sand) are much different from the rest of the five sand soils (host sands) tested. In Table 3, the 20 sandy soils are classified following the Unified Soil Classification System (ASTM 2011). The values of threshold fines content (FC_{th}) in Table 3 were estimated using the formula of Rahman et al. (2009).

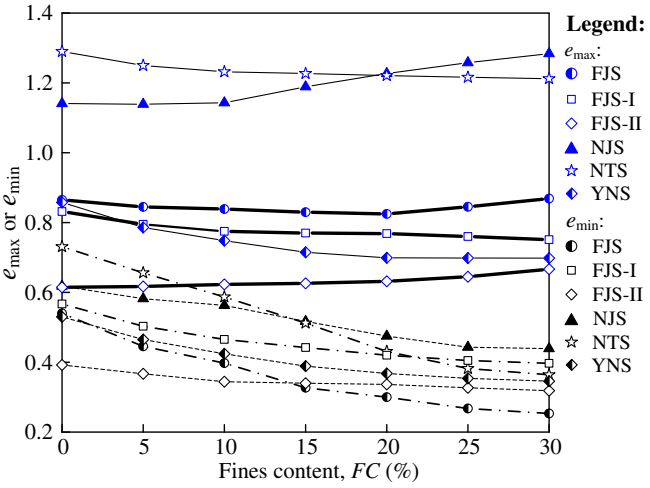

Fig. 2. Maximum and minimum void ratios of six sandy soils with various nonplastic FC tested in this study.

Specimen Preparation, Saturation, and Consolidation

For the CTX tests, all specimens of the sandy soils were prepared by the moist tamping method using an undercompaction procedure according to ASTM D3999/D3999M (ASTM 2013). Note that the liquefaction resistance of soils is highly dependent on the degree of saturation (Yang et al. 2004); a two-stage saturation (carbon dioxide flushing and deaired water flushing) was carried out carefully, followed by back pressure saturation at the back pressure of 400 kPa. A Skempton's B-value of 0.95 or larger was considered acceptable. After saturation, all the specimens were isotropically consolidated to the σ'_{c0} of 100 kPa.

The BE tests were conducted on specimens with a diameter of 100 mm and length of 200 mm at the isotropic consolidation condition, for which the process of specimen preparation, saturation, and consolidation were the same as for the CTX tests.

Testing Program and Process

The stress-controlled undrained CTX tests were performed following the cyclic loading procedures outlined in the ASTM test standard (ASTM 2013). CSR is defined as the ratio of the half-amplitude of uniform cyclic axial stress ($\sigma_d/2$) to the σ'_{c0} in this paper. The cell pressure was held constant, while the sinusoidal, double-amplitude uniform cyclic loadings were applied with a frequency of 1 Hz at various CSRs ranging from 0.063 to 0.458.

Table 2. Index properties of host sands and pure fines for six sandy soils tested in this study and 14 sandy soils from the literature

Material ID	Data from	Matertial: Host sand + pure fines	Index property: e^s_{max}/e^f_{max}	e^s_{min}/e^f_{min}	d^s_{50}/d^f_{50} (mm)	d^s_{10}/d^f_{10} (mm)	C^s_u/C^f_u	e^s_{range}/e^f_{range}	χ
M1	Chang and Hong (2008)	Vietnam fine silica sand + Kaolinite soil	0.92/N.D.	0.62/N.D.	0.500/0.0046	0.282/0.0012	2.01/5.42	0.31/N.D.	61.3
M2	Dash et al. (2010) and Sitharam et al. (2013)	Ahmedabad sand + Bangalore quarry dust	0.68/1.63	0.42/0.52	0.375/0.0371	0.121/N.D.	3.58/7.83	0.26/0.98	3.2
M3	Huang et al. (2004)	Mailiao sand + Mailiao silt	1.13/N.D.	0.65/N.D.	0.126/0.0423	0.083/0.0171	1.67/2.94	0.48/N.D.	2.0
M4	Kim et al. (2016)	Mikawa silica sand + Iwakuni marine clay	0.85/N.D.	0.52/N.D.	0.887/0.0061	0.289/0.0015	3.60/5.56	0.33/N.D.	48.2
M5	Kuerbis (1989)	Brenda Mine tailings sand + Kamloops silt	0.86/2.67	0.52/1.45	0.250/0.0119	0.093/0.0043	3.44/3.09	0.35/1.22	7.8
M6	Papadopoulou and Tika (2008)	Greece Assyros quartz sand + Assyros silt	0.84/1.66	0.58/0.66	0.300/0.0201	0.228/0.0043	1.30/7.50	0.26/1.00	11.4
M7	Stamatopoulos (2010)	Egyptian quartz sand + Greece quartz silt	0.84/1.66	0.55/0.66	0.359/0.0201	0.172/0.0043	2.43/6.50	0.29/1.00	8.6
M8	Polito and Martin (2001)	Monterey No. 0/30 sand + Yatesville silt	0.82/1.72	0.63/0.74	0.430/0.0317	0.310/0.0088	1.55/4.39	0.19/0.98	9.7
M9	Polito and Martin (2001)	Yatesville sand + Yatesville silt	0.97/1.72	0.65/0.74	0.180/0.0317	0.089/0.0088	2.45/4.39	0.32/0.98	2.8
M10	Payan et al. (2017)	White sand + silica silt	N.D./N.D.	N.D./N.D.	0.247/0.0143	0.158/0.0017	1.73/10.12	N.D./N.D.	11.3
M11	Payan et al. (2017)	Blue sand 2 + silica silt	N.D./N.D.	N.D./N.D.	1.836/0.0143	0.587/0.0017	3.82/10.12	N.D./N.D.	41.9
M12	Goudarzy et al. (2016)	Hostun sand + quartz powder	1.02/N.D.	0.67/N.D.	0.338/0.0028	0.190/0.0008	2.01/4.76	0.35/N.D.	65.5
M13	Wichtmann et al. (2015)	Dorsten sand + quartz powder	1.11/N.D.	0.67/N.D.	0.100/0.0089	0.080/0.0032	1.30/9.01	0.43/N.D.	8.9
M14	Yang and Liu (2016)	Toyoura sand + silica silt	N.D./N.D.	N.D./N.D.	0.216/0.0543	0.166/0.0279	1.39/2.18	N.D./N.D.	3.1
M15	This study	Fujian sand + Nantong silt (FJS)	0.87/1.53	0.54/0.83	0.361/0.0348	0.116/0.0158	3.79/2.95	0.32/0.90	3.3
M16	This study	Fujian sand - I + Nantong silt (FJS-I)	0.83/1.53	0.57/0.83	0.330/0.0348	0.130/0.0158	2.89/2.95	0.26/0.90	3.7
M17	This study	Fujian sand - II + Nantong silt (FJS-II)	0.61/1.53	0.39/0.83	0.350/0.0348	0.090/0.0158	11.11/2.95	0.22/0.90	2.6
M18	This study	Nanjing sand + Nantong silt (NJS)	1.14/1.53	0.62/0.83	0.169/0.0348	0.105/0.0158	2.31/2.95	0.52/0.90	3.0
M19	This study	Nantong sand + Nantong silt (NTS)	1.29/1.53	0.73/0.83	0.113/0.0348	0.080/0.0158	1.65/2.95	0.56/0.90	2.3
M20	This study	Yunnan sand + Nantong silt (YNS)	0.86/1.53	0.53/0.83	1.265/0.0348	0.869/0.0158	1.64/2.95	0.33/0.90	24.8

Note: N.D. = no description; d_{10}, d_{50}, and d_{60} = particle sizes corresponding to 10%, 50%, and 60% finer on the cumulative particle-size distribution curve, respectively; uniformity coefficient, $C_u = d_{60}/d_{10}$; void ratio range, $e_{range} = e_{max} - e_{min}$; superscripts s and f denote host sand and pure fines, respectively; and $\chi = d^s_{10}/d^f_{50}$.

Table 3. Basic information on the undrained CS, CTX, RC, and/or BE tests of six sandy soils in this study and 14 sandy soils from the literature

Material ID	Preparation method	Sample size/mm (diameter × height)	Test category		FC (%)	σ'_{c0} (kPa)	Liquefaction criterion	FC_{th} (%)	b value	Group symbol (USCS)
			CRR	V_s						
M1	MT	25 × 68	CS		0–15	100	$\gamma_{da} = 6\%$	40.6	0–0.343	SP, SP-SM, SM
M2	DR	50 × 100	CTX		0–30	100	$\varepsilon_{da} = 5\%$	31.6	0–0.475	SP, SP-SM,
M3	MT/WS/DR	50 × 100	CTX	BE	0–30	100	$r_u = 1$	42.5	0–0.502	SP, SM,
M4	MT	50 × 100	CS		0–16.7	100	$\gamma_{da} = 5\%$	40.0	0–0.349	SP, SW-SC, SC
M5	SD	N.D.	CTX		0–13.5	350	$\varepsilon_{sa} = 2.5\%$	30.6	0–0.354	[a]
M6	MT	50 × 100	CTX		0–25	100	$\varepsilon_{da} = 5\%$	32.6	0–0.381	[a]
M7	MT	38.2 × 84.9	CTX		0–25	50, 100, 150, 200	$\varepsilon_{da} = 5\%$	30.6	0–0.391	SP, SM
M8	N.D.	71 × 154	CTX		0–25	100	$r_u = 1$	31.4	0–0.386	SP, SP-SM, SM
M9	N.D.	71 × 154	CTX		0–26	100	$r_u = 1$	33.1	0–0.468	SP, SP-SM, SM
M10	DR	50 × 100		RC	0–30	50, 100, 200, 400, 800		32.6	0–0.387	SP, SP-SM, SM
M11	DR	50 × 100		RC	0–30	50, 100, 200, 400, 800		40.7	0–0.354	SP, SP-SM, SM
M12	DR	100 × 200		BE	0–40	80, 110, 140, 170, 200		40.6	0–0.346	SP, SP-SM, SM
M13	DR	100 × 200		RC	0–19.6	50, 70, 100, 150, 200, 300, 400		39.6	0–0.358	SP, SP-SM, SM
M14	MT	50 × 100		BE	0–30	100, 200, 400, 500		32.0	0–0.480	SP, SP-SM, SM
M15	MT	50 × 100 for CTX 100 × 200 for BE	CTX	BE	0–30	100	$r_u = 1$	31.4	0–0.472	SP, SW-SM, SM
M16	MT	50 × 100 for CTX 100 × 200 for BE	CTX	BE	0–30	100 for CTX/100, 200, 300 for BE	$r_u = 1$	30.6	0–0.436	SW, SP-SM, SM
M17	MT	50 × 100 for CTX/100 × 200 for BE	CTX	BE	0–30	100 for CTX/100, 200, 300 for BE	$r_u = 1$	33.9	0–0.502	SP, SP-SM, SM
M18	MT	50 × 100 for CTX 100 × 200 for BE	CTX	BE	0–30	100	$r_u = 1$	32.2	0–0.483	SP, SP-SM, SM
M19	MT	50 × 100 for CTX 100 × 200 for BE	CTX	BE	0–30	100	$r_u = 1$	35.5	0–0.517	SP, SP-SM, SM
M20	MT	50 × 100 for CTX 100 × 200 for BE	CTX	BE	0–30	100 for CTX/100, 200, 300 for BE	$r_u = 1$	39.2	0–0.365	SP, SP-SM, SM

Note: DR = dry deposition; MT = moist tamping; WS = water sedimentation; SD = slurry deposition; CTX = cyclic triaxial test; CS = cyclic shear test; BE = bender element test; RC = resonant column test; ε_{da} = double-amplitude axial strain; γ_{da} = double-amplitude shear strain; ε_{sa} = single amplitude axial strain; and N.D. = no description.

[a]Cannot be determined from the data in the literature cited.

Note that the conflicting views about the effect of nonplastic fines on the liquefaction susceptibility of sandy soils may be due to the use of different state variables as the comparison basis (Yang et al. 2015). The tests of FJS, NJS, and NTS are divided into three groups with the same target initial D_r, the same target initial e; and the same target initial skeleton void ratio (e_{sk}). The tests of FJS-I, FJS-II, and YNS are divided into two groups with the target initial $D_r = 50\%$ and $D_r = 70\%$. The maximum deviations of the actual D_r values of specimens after consolidation from the target initial $D_r = 50\%$ and $D_r = 70\%$ are less than 2.5% and 3.7%, respectively. The maximum relative deviations of the actual e and e_{sk} values of specimens after consolidation from their target initial values are less than 2.1% and 2.0%, respectively. All 76 cases are listed in Table 4. Fig. 3 illustrates the typical time histories of r_u and axial strain (ε_a) for the CTX test results of six sandy soils.

For each BE test, a set of sinusoid signals from 1 to 40 kHz, rather than a single signal, was used as the excitation, and the received signals corresponding to these excitation frequencies were examined in whole to better identify the travel time of the shear wave (Yang and Gu 2013). The 10-kHz excitation signal was found to consistently yield a clear arrival of the shear wave for both clean sands and sandy soils. This is in good agreement with the observation of Yang and Liu (2016). Fig. 4 presents typical signal capture for the four sandy soils from the BE tests. The determination of the shear-wave travel time using the first arrival has been used by many researchers (e.g., Huang et al. 2004; Baxter et al. 2008). Among them, 52 cases for FJS, NJS, and NTS were tested under the σ'_{c0} of 100 kPa in a single stage, while the other 24 cases for FJS-I, FJS-II, and YNS were tested under the σ'_{c0} of 100, 200, and 300 kPa in three stages.

Binary Packing State Parameter

The intergrain state concept (Evans and Zhou 1995; Thevanayagam et al. 2002; Xenaki and Athanasopoulos 2003; Chen et al. 2018) is adopted herein to interpret the behavior of granular soil under undrained CTX loading. For the binary packing system, the $e_{\min}$ is reached when the voids in the primary fabric of coarse particles are completely filled with fine particles. When the fines are fully present within the void spaces between the coarse matrix, fines are assumed to make no contribution to the load-transferring skeleton. The FC_{th} has been introduced to distinguish the regime of *fines in coarse* (coarse-material-dominated behavior) from *coarse in fines* (fines-material-dominated behavior) soil mixtures (Thevanayagam et al. 2002; Rahman and Lo 2008; Rahman et al. 2011). The FC_{th} can be determined by the empirical equation (Rahman et al. 2009)

$$FC_{th} = 0.40 \times \left[\frac{1}{1+\exp(\alpha-\beta\chi)} + \frac{1}{\chi}\right] \tag{1}$$

where $\alpha = 0.50$ and $\beta = 0.13$ are curve-fitting constants; and χ = the particle-size disparity ratio, $\chi = d_{10}^{s}/d_{50}^{f}$.

For a binary packing system, fines completely contained within the void space are thought to make no contribution to the observed behavior. Thus, by neglecting the fines, an index known as the skeleton void ratio e_{sk} is used as an alternative to characterize the state of the mixtures of sand particles and fines (Thevanayagam 2000; Thevanayagam et al. 2002; Rahman et al. 2011; Chen et al. 2018). With an increase in FC, fines may come in between the contact of sand grains and participate in the force chain. Thus, the effect of fines on the force transfer mechanism is considered by introducing an alternative equivalent skeleton void ratio (e^*_{sk}) to replace the e_{sk}, as defined by Eq. (2) (Thevanayagam et al. 2002)

$$e^*_{sk} = \frac{e + (1-b)\cdot FC}{1-(1-b)\cdot FC} \tag{2}$$

The physical meaning of b is the fraction of fines that are active in the force chain between soil grains. The rationale behind Eq. (2) requires coarse-material-dominated behavior. This meaning of b requires $\mathrm{FC} < FC_{th}$ and $0 \le b < 1$. Note that $b = 0$ leads to $e^*_{sk} = e_{sk}$. The value of b is empirically estimated using the equation (Mohammadi and Qadimi 2015)

$$b = \left\{1 - \exp\left(-\frac{0.3}{k}\right)\right\}\left(r \times \frac{FC}{FC_{th}}\right)^r \tag{3}$$

where $r = 1/\chi$ and $k = 1 - r^{0.25}$. Note that the e values used in this paper are the measured values after consolidation.

CTX Testing Results and CRR Prediction Equation

Factors Influencing CRR

As seen in Fig. 3, the oscillation amplitude of ε_a keeps increasing in a low rate until r_u exceeds 0.8, after which the oscillation amplitude is enlarged dramatically toward initial liquefaction in the next several cycles. Thus, r_u of 100% is adopted as the criterion for the initial liquefaction of sandy soils in this study.

The cyclic resistance curves of sandy soils are expressed as the measured CSR versus the number of cycles (N_1) required to cause r_u of 100%. Fig. 5 presents the CSR–N_1 relationships of the six sandy soils tested. In general, the N_1 decreases with increasing CSR for the six sandy soils. For each host sand, the CSR-log N_1 curves with various FC and densities are nearly parallel to each other. The changes in the physical state indices and index properties of sandy soils only lead to a shift of the CSR-log N_1 curve upward or downward, but generally do not change the shape of the CSR-log N_1 curve.

A common assumption that an M_w 7.5 earthquake can be simulated by 15 uniform loading cycles is adopted, and the CRR in 15 cycles is denoted as CRR_{15}. Fig. 6 shows the variations of the measured CRR_{15} with varying FC for three physical state variables: D_r, e, and e_{sk}. It can be seen that CRR_{15} significantly decreases with an increase in FC for the same target initial values of D_r or e; but conversely, an increase in the CRR_{15} is consistent with an increase in FC for the same target initial values of e_{sk}.

Both physical state variables and material properties have a governing influence on the undrained cyclic resistance and deformation characteristics of sandy soils. It is thus interesting to examine the influence of D_r, e, or e_{sk}; mean particle size (d_{50}); uniformity coefficient (C_u); and void ratio range ($e_{\mathrm{range}} = e_{\max} - e_{\mathrm{main}}$) on the measured CRR_{15}. Fig. 7 shows the variations of the CRR_{15} with the D_r, e, or e_{sk} of all specimens after consolidation for FJS, NJS, and NTS (Table 4). It is noted that the correlation between CRR_{15} and any variable among D_r, e, or e_{sk} is greatly influenced by FC. Fig. 8 shows the test results with various material properties d_{50}, C_u, and e_{range} for FJS, NJS, and NTS (Table 4). There is no universal variation tendency of CRR_{15} with any of d_{50}, C_u, and e_{range}. Therefore, any single index of the physical state variables and of the material properties is not able to characterize in a unified way the liquefaction resistance of sandy soils. It is desirable to search for an alternative proxy that can characterize in a unified model the liquefaction resistance.

CRR Prediction Equation

Fig. 9 presents the relationships between CRR_{15} and e^*_{sk} for the tested six sandy soils. Despite larger differences in physical state

Table 4. Schemes of the undrained CTX and BE tests on isotropically consolidated specimens for six sandy soils in this study

Case ID							Case ID							Case ID						
CTX test	BE test	FC (%)	D_r (%)	e	e_{sk}	σ'_{c0} (kPa)	CTX test	BE test	FC (%)	D_r (%)	e	e_{sk}	σ'_{c0} (kPa)	CTX test	BE test	FC (%)	D_r (%)	e	e_{sk}	σ'_{c0} (kPa)
FJS-1	FJS-19	0	50	0.70	0.70	100[a]	NJS-1	NJS-19	0	50	0.88	0.88	100[a]	NJS-1	NJS-19	0	50	1.01	1.01	100[a]
FJS-2	FJS-20	10	50	0.62	0.80		NJS-2	NJS-20	10	50	0.85	1.06		NJS-2	NJS-20	10	50	0.91	1.12	
FJS-3	FJS-21	15	50	0.58	0.86		NJS-3	NJS-21	15	50	0.85	1.18		NJS-3	NJS-21	15	50	0.87	1.20	
FJS-4	FJS-22	20	50	0.56	0.95		NJS-4	NJS-22	20	50	0.85	1.31		NJS-4	NJS-22	20	50	0.83	1.28	
FJS-5	FJS-23	25	50	0.56	1.08		NJS-5	NJS-23	25	50	0.85	1.47		NJS-5	NJS-23	25	50	0.80	1.40	
FJS-6	FJS-24	30	50	0.56	1.23		NJS-6	NJS-24	30	50	0.86	1.66		NJS-6	NJS-24	30	50	0.79	1.55	
FJS-7	FJS-25	0	60.0	0.67	0.67		NJS-7	NJS-25	0	27.0	1.00	1.00		NJS-7	NJS-25	0	76.9	0.86	0.86	
FJS-8	FJS-26	10	38.2	0.67	0.86		NJS-8	NJS-26	10	24.7	1.00	1.22		NJS-8	NJS-26	10	57.7	0.86	1.07	
FJS-9	FJS-27	15	31.8	0.67	0.96		NJS-9	NJS-27	15	28.1	1.00	1.35		NJS-9	NJS-27	15	51.3	0.86	1.19	
FJS-10	FJS-28	20	29.5	0.67	1.09		NJS-10	NJS-28	20	30.2	1.00	1.50		NJS-10	NJS-28	20	45.7	0.86	1.33	
FJS-11	FJS-29	25	30.3	0.67	1.23		NJS-11	NJS-29	25	31.7	1.00	1.67		NJS-11	NJS-29	25	42.7	0.86	1.48	
FJS-12	FJS-30	30	32.3	0.67	1.39		NJS-12	NJS-30	30	33.6	1.00	1.86		NJS-12	NJS-30	30	41.5	0.86	1.66	
FJS-13[b]	FJS-31	0	—	—	—		NJS-13[b]	NJS-31	0	—	—	—		NJS-13	NJS-31	0	25.0	1.15	1.15	
FJS-14	FJS-32	10	19.0	0.76	0.95		NJS-14	NJS-32	10	20.3	1.03	1.25		NJS-14	NJS-32	10	46.0	0.94	1.15	
FJS-15	FJS-33	15	34.3	0.66	0.95		NJS-15	NJS-33	15	41.1	0.91	1.25		NJS-15	NJS-33	15	55.9	0.83	1.15	
FJS-16	FJS-34	20	50.5	0.56	0.95		NJS-16	NJS-34	20	56.8	0.80	1.25		NJS-16	NJS-34	20	63.4	0.72	1.15	
FJS-17	FJS-35	25	66.2	0.46	0.95		NJS-17	NJS-35	25	70.0	0.69	1.25		NJS-17	NJS-35	25	72.4	0.61	1.15	
FJS-18	FJS-36	30	81.8	0.37	0.95		NJS-18	NJS-36	30	83.9	0.58	1.25		NJS-18	NJS-36	30	83.4	0.51	1.15	
FJS-I−1	FJS-I−9	0	50	0.70	0.70		FJS-II−1	FJS-II−9	0	50	0.50	0.50		YNS-1	YNS-9	0	50	0.69	0.69	
FJS-I−2	FJS-I−10	10	50	0.62	0.80		FJS-II−2	FJS-II−10	10	50	0.48	0.65		YNS-2	YNS-10	10	50	0.59	0.76	
FJS-I−3	FJS-I−11	20	50	0.59	0.99	100[c]	FJS-II−3	FJS-II−11	20	50	0.48	0.86	100	YNS-3	YNS-11	20	50	0.53	0.92	100[c]
FJS-I−4	FJS-I−12	30	50	0.57	1.25	200[c]	FJS-II−4	FJS-II−12	30	50	0.49	1.13	200	YNS-4	YNS-12	30	50	0.52	1.17	200[c]
FJS-I−5	FJS-I−13	0	70	0.65	0.65	300[c]	FJS-II−5	FJS-II−13	0	70	0.46	0.46	300[c]	YNS-5	YNS-13	0	70	0.63	0.63	300[c]
FJS-I−6	FJS-I−14	10	70	0.56	0.73		FJS-II−6	FJS-II−14	10	70	0.43	0.59		YNS-6	YNS-14	10	70	0.52	0.69	
FJS-I−7	FJS-I−15	20	70	0.52	0.91		FJS-II−7	FJS-II−15	20	70	0.43	0.78		YNS-7	YNS-15	20	70	0.47	0.83	
FJS-I−8	FJS-I−16	30	70	0.50	1.15		FJS-II−8	FJS-II−16	30	70	0.42	1.03		YNS-8	YNS-16	30	70	0.45	1.07	

[a]100 kPa for both CTX and BE tests.
[b]The estimated e is over e_{max}.
[c]100 kPa for CTX tests and 100, 200, and 300 kPa for BE tests.

Table 5. Index properties of host sands and pure fines for five sandy soils compiled from the literature for independent validation

Material ID	Data from	Matertial: Host sand + pure fines	Index property: e^s_{max}/e^f_{max}	e^s_{min}/e^f_{min}	d^s_{50}/d^f_{50} (mm)	d^s_{10}/d^f_{10} (mm)	C^s_u/C^f_u	e^s_{range}/e^f_{range}	χ
VM1	Hsiao et al. (2015)	Taiwan clean sand + Taiwan pure silt	0.70/N.D.	0.24/N.D.	0.636/0.015	0.113/0.0034	7.92/2.50	0.46/N.D.	7.5
VM2	Xenaki and Athanasopoulos (2003)	Greece sand + Greece silt	1.05/1.70	0.66/0.66	0.120/0.020	0.083/0.0067	1.63/4.43	0.38/1.05	4.2
VM3	Akhila et al. (2019)	India fine sand + crush stone power	0.86/0.58	N.D./N.D.	0.280/0.011	0.121/0.0041	2.63/4.08	0.28/N.D.	12.0
VM4	Payan et al. (2017)	Blue sand 1 + Silica silt	N.D./N.D.	N.D./N.D.	0.698/0.014	0.375/0.0017	2.06/10.10	N.D./N.D.	26.8
VM5	Salgado et al. (2000)	Ottawa sand + Sil-Co-Sil ground silica	0.78/N.D.	0.48/N.D.	0.386/0.0229	0.266/0.0014	1.48/22.78	0.30/N.D.	11.6

Note: N.D. = no description.

Table 6. Basic information on the undrained CTX, RC, and BE tests for five sandy soils from the literature for independent validation

Material ID	Preparation method	Sample size/mm (diameter × height)	Test category: CRR	Test category: V_s	FC (%)	σ'_{c0} (kPa)	Liquefaction criterion	FC (%)	b value	Group symbol (USCS)
VM1	MT	71 × 150	CTX	—	0–30	100	$r_u = 1$	30.0	0–0.432	SP, SC-SM,
VM2	DR	50 × 115	CTX	—	30	200	$r_u = 1$	30.1	0.448	SM
VM3	MT	50 × 100	CTX	—	0–30	100	$r_u = 1$	30.4	0–0.340	SP, SP-SM, SM
VM4	DR	50 × 100	—	RC	0–30	50, 100, 200, 400, 800	—	39.6	0–0.363	SP, SP-SM, SM
VM5	SD	70 × 165	—	BE	0–20	100	—	32.8	0–0.466	SP, SP-SM, SM

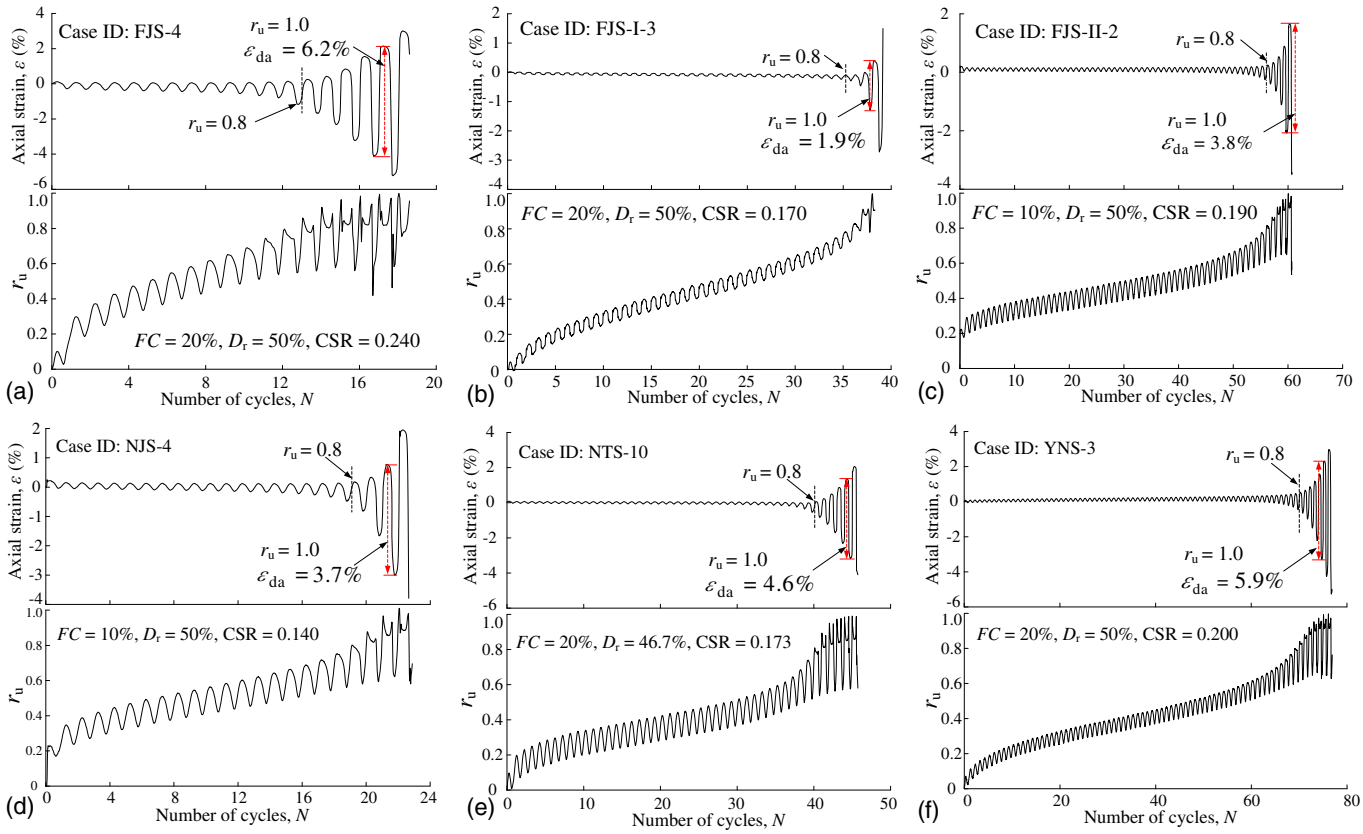

Fig. 3. Typical undrained CTX test results on six sandy soils in this study for case ID: (a) FJS-4; (b) FJS-I-3; (c) FJS-II-2; (d) NJS-4; (e) NTS-10; and (f) YNS-3.

(D_r, e, e_{sk}) and material properties (d_{50}, C_u, FC, e_{range}), all test data points of each sandy soil are located in a relatively narrow band. This indicates that the form of the relationships between CRR_{15} and e^*_{sk} for sandy soils with various d_{50}, C_u, D_r, e, e_{sk}, and FC is unique. The parameters entering the relationships are soil-specific but, as will be shown later, can be determined by a single set of equations. Remarkably, compared with any single index of the material properties or the physical state variables, e^*_{sk} is a more

J. Geotech. Geoenviron. Eng., 2020, 146(6): 04020040

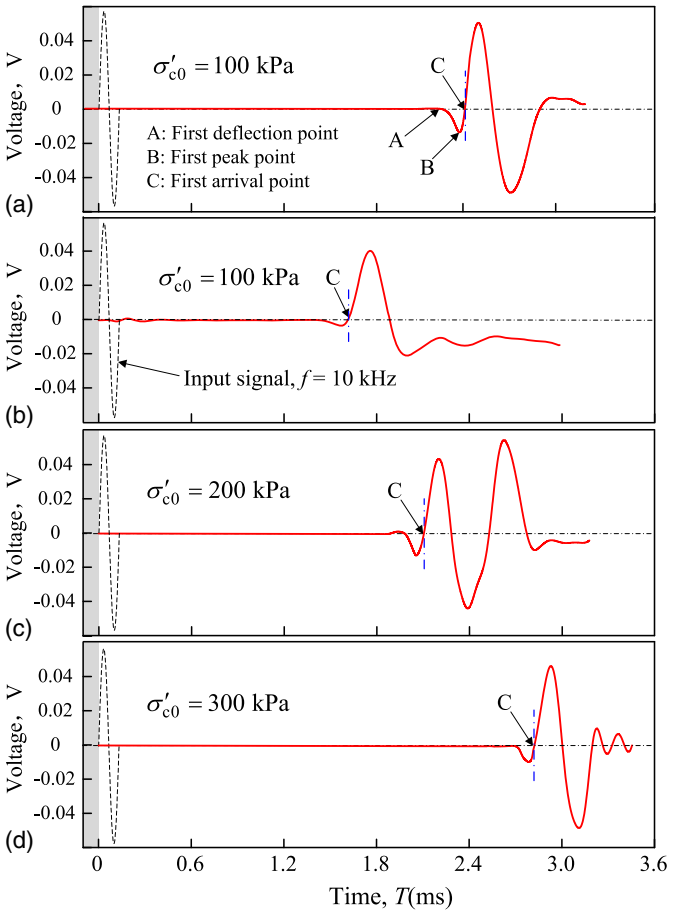

Fig. 4. Typical time histories of input and output signals from bender element tests.

rational proxy to characterize the liquefaction resistance. To further examine the applicability of the new proxy, the independent test data of nine sandy soils in the literature (Table 2) were collected and analyzed. All of the (CRR_{15}, e^*_{sk}) data pairs under the variety of d_{50}, C_u, D_r, e, e_{sk}, FC, and σ'_{c0} are plotted in Fig. 10. All of the cyclic laboratory tests for the nine sandy soils reported in the literature were conducted under isotropically consolidated condition. It is striking that all data points for each of the nine sandy soils now fall within a very narrow band, suggesting that a unique form of the relationships exists between CRR_{15} and e^*_{sk} regardless of the d_{50}, C_u, D_r, e, e_{sk}, FC, and σ'_{c0}. Therefore, the e^*_{sk} appears to adequately capture the effects of the nature of material properties, density, and particle gradations if FC < FC_{th}. In this regard, e^*_{sk} is an appropriate proxy to characterize the cyclic liquefaction resistance for sandy soils. Furthermore, based on the plots in Figs. 9 and 10, a unified model between CRR_{15} and e^*_{sk} follows a negative power law

$$CRR_{15} = A_1(e^*_{sk})^{-B_1} \tag{4}$$

where parameters A_1 and B_1 are assumed to be material-dependent best-fitting constants.

Using a generalized nonlinear regression model for the experimental data of 15 sandy soils, the parameters A_1 and B_1 are related to the binary material property parameters as follows (Fig. 11):

$$A_1 = C_1[\sqrt{C^s_u}C^f_u/(10e^s_{\text{range}})]^{C_2} \tag{5}$$

$$B_1 = C_3\left(\frac{d^s_{50}}{d_{th}\sqrt{\chi}}\right)^2 + C_4\left(\frac{d^s_{50}}{d_{th}\sqrt{\chi}}\right) + C_5 \tag{6}$$

where C_1 and C_2 = best-fitting coefficients for set of [A_1, $\sqrt{C^s_u}C^f_u/(10e^s_{\text{range}})$] data points, $C_1 = 0.195$, $C_2 = -0.651$; C_3, C_4, and C_5 = best-fitting coefficients for set of [B_1, $d^s_{50}/(d_{th}\sqrt{\chi})$] data points, $C_3 = -1.291$, $C_4 = 4.895$, $C_5 = -1.492$; correspondingly,

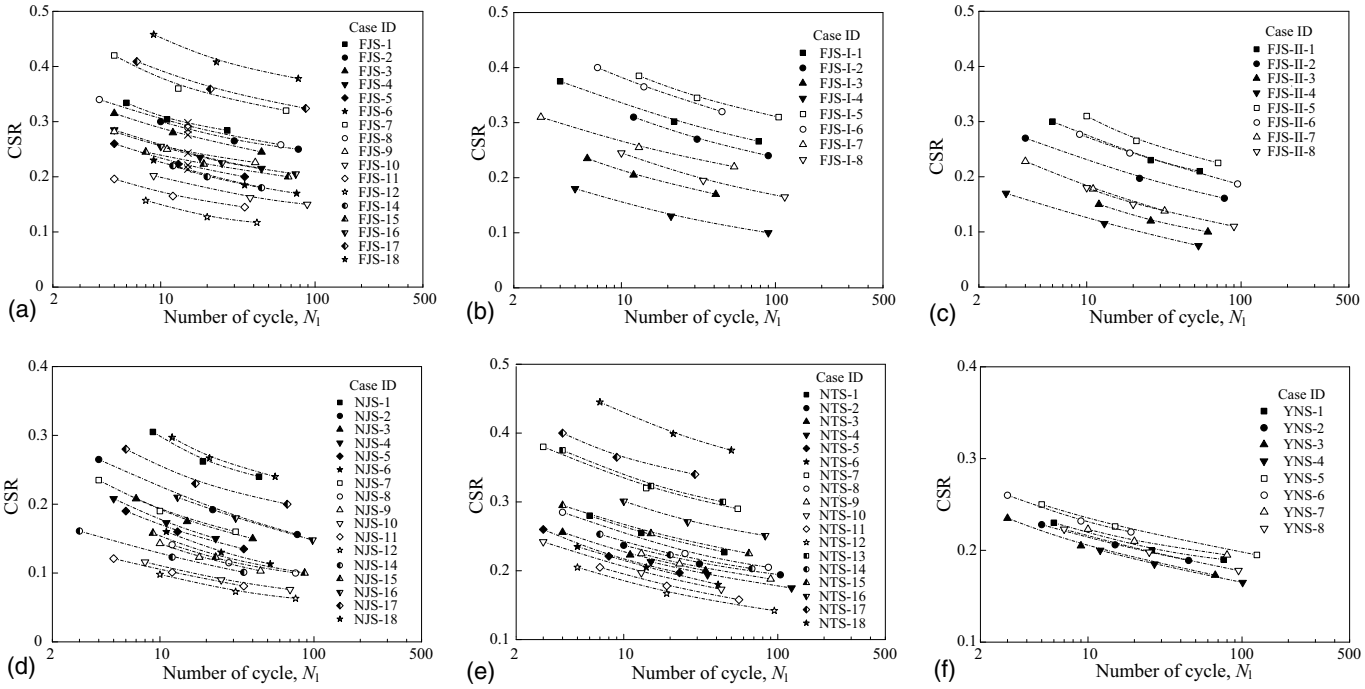

Fig. 5. Relationships between the measured CSR and the number of cycles N_l required to cause initial liquefaction for six sandy soils: (a) FJS; (b) FJS-I; (c) FJS-II; (d) NJS; (e) NTS; and (f) YNS.

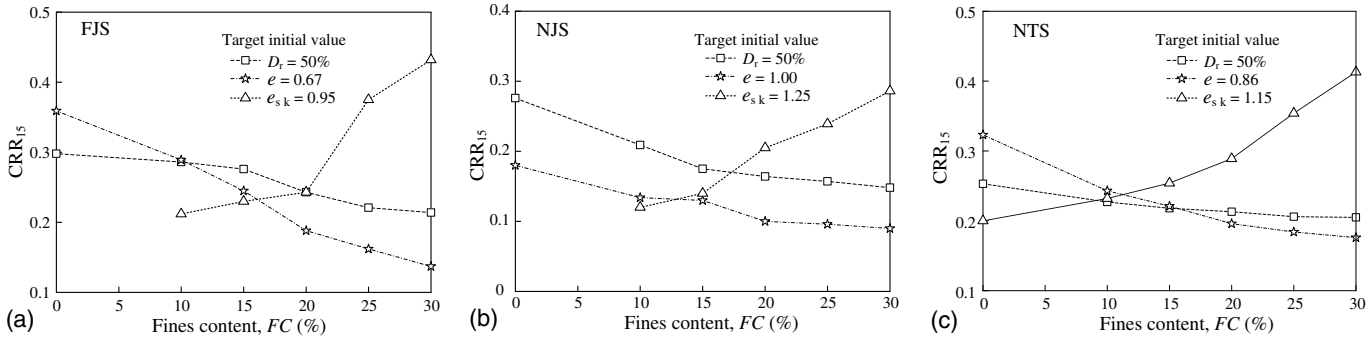

Fig. 6. Variation of CRR_{15} of a sandy soil with FC for given target initial values of D_r, e, and e_{sk}: (a) FJS; (b) NJS; and (c) NTS.

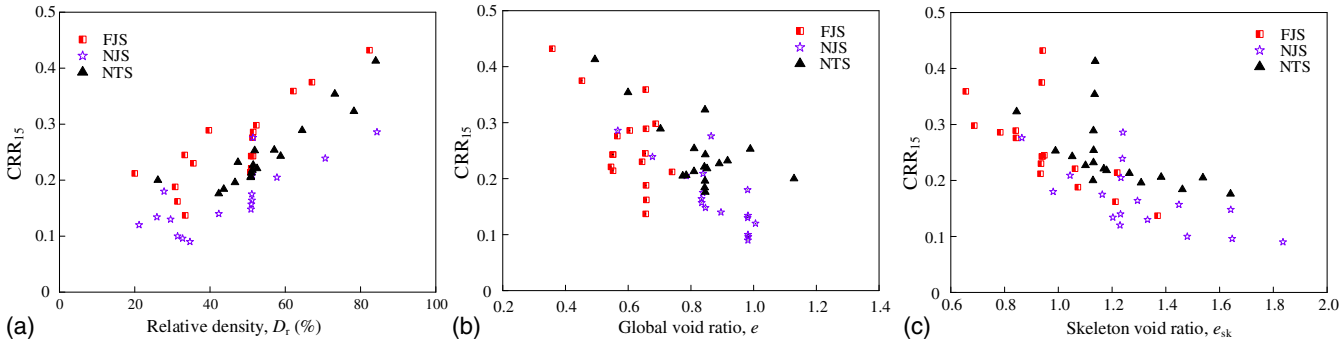

Fig. 7. Variation of CRR_{15} with D_r, e, or e_{sk} for FJS, NJS, and NTS: (a) CRR_{15} versus D_r; (b) CRR_{15} versus e; and (c) CRR_{15} versus e_{sk}.

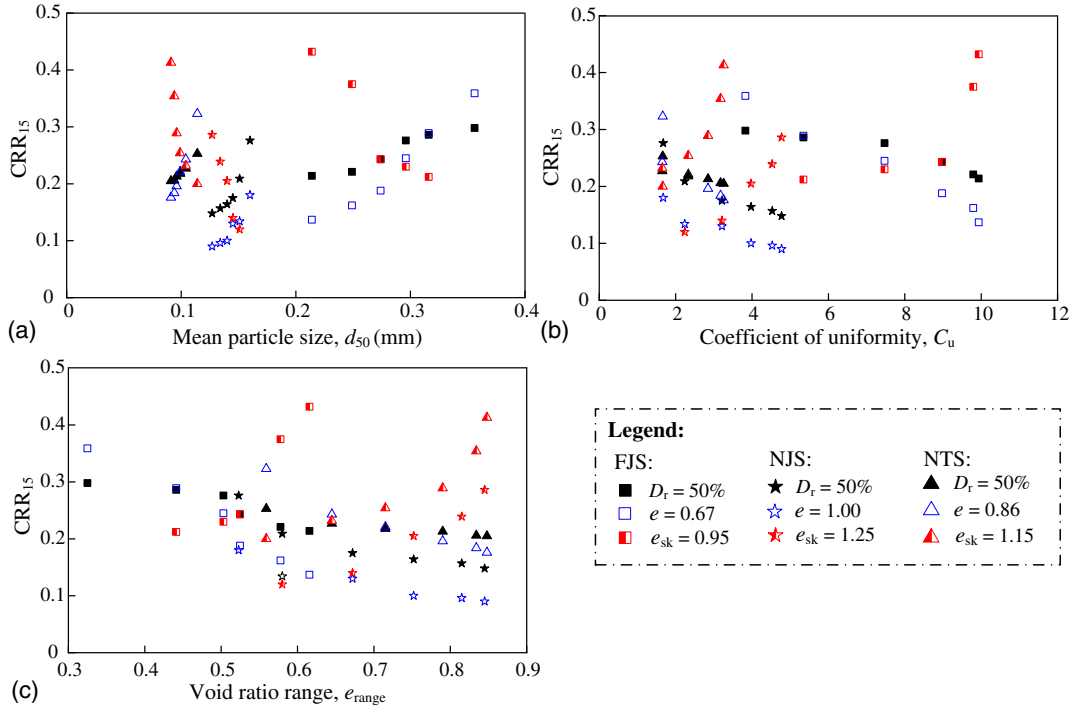

Fig. 8. Variation of CRR_{15} with d_{50}, C_u, and e_{range} for FJS, NJS, and NTS: (a) CRR_{15} versus d_{50}; (b) CRR_{15} versus C_u; and (c) CRR_{15} versus e_{range}.

the R-square value of a nonlinear regression for Eqs. (5) and (6) is 0.98 and 0.97, respectively; d_{th} = limiting particle size (0.075 mm) distinguishing the regime of sand from fines.

Although the particle natures of the six sandy soils tested in this study and the nine sandy soils in the literature are differing and the physical state indices and material properties vary greatly, the corresponding R-square values of the nonlinear regression models are still greater than 0.97. Therefore, the coefficients C_1–C_5 can be assumed to be constant independent of the type of sandy soil, and the relationship in Eq. (4) can be used to predict in a simple yet reliable

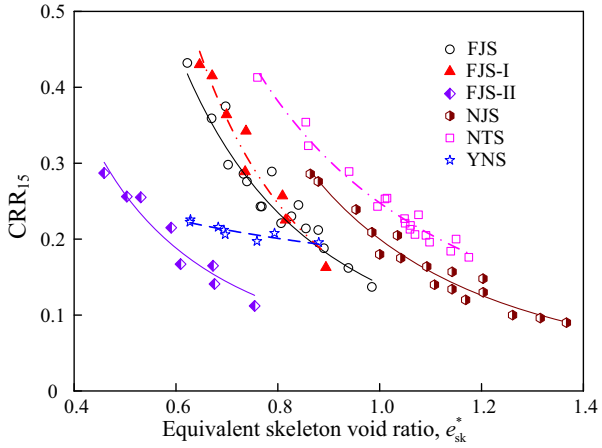

Fig. 9. Relationships between CRR_{15} and e^*_{sk} for six sandy soils tested in this study.

way the cyclic liquefaction resistance of a wide range of sandy soils when FC is less than FC_{th}.

BE Testing Results and V_s Prediction Equation

The measured V_s in the field or the laboratory is corrected to 1 atm reference confining pressure (Andrus and Stokoe 2000; Youd et al. 2001):

$$V_{s1} = V_s C_V = V_s (P_a/\sigma'_{c0})^{0.25} \tag{7}$$

where V_{s1} = confining-pressure-corrected shear-wave velocity; C_V = factor to correct the measured V_s for effective overburden pressure, P_a = atmospheric pressure (100 kPa); and σ'_{c0} = the effective isotropic confining pressure of the measured V_s. For convenience, $V_{s\text{-lab}}$ and $V_{s\text{-field}}$ are denoted as the measured V_s in the laboratory and in the field, respectively. Correspondingly, $V_{s1\text{-lab}}$

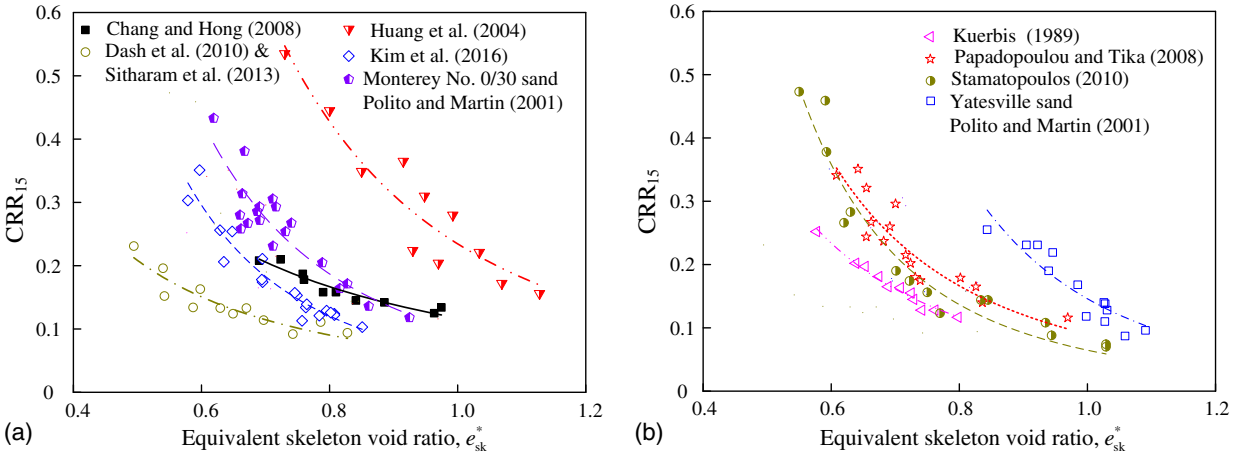

Fig. 10. Relationships between CRR_{15} and e^*_{sk} for nine sandy soils using compiled data from the literature: (a) the undrained tests of Huang et al. (2004), Polito and Martin (2001), Chang and Hong (2008), Dash et al. (2010), Sitharam et al. (2013), and Kim et al. (2016); and (b) the undrained tests of Kuerbis (1989), Polito and Martin (2001), Papadopoulou and Tika (2008), and Stamatopoulos (2010.)

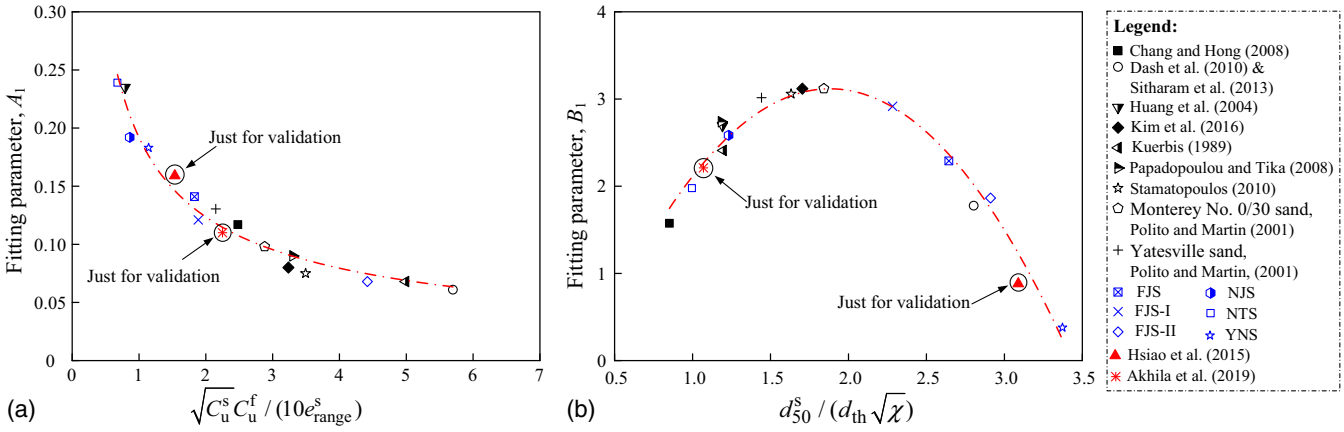

Fig. 11. Relationships between parameters A_1, B_1 and the binary material parameters for six sandy soils in this study and nine sandy soils using compiled data from the tests of Kuerbis (1989), Polito and Martin (2001), Huang et al. (2004), Chang and Hong (2008), Papadopoulou and Tika (2008), Dash et al. (2010), Sitharam et al. (2013), Stamatopoulos (2010), and Kim et al. (2016), as well as validations using compiled data from the tests of Hsiao et al. (2015) and Akhila et al. (2019): (a) A_1 versus $\sqrt{C^s_u C^f_u}/(10e^s_{\text{range}})$; and (b) B_1 versus $d^s_{50}/(d_{th}\sqrt{\chi})$.

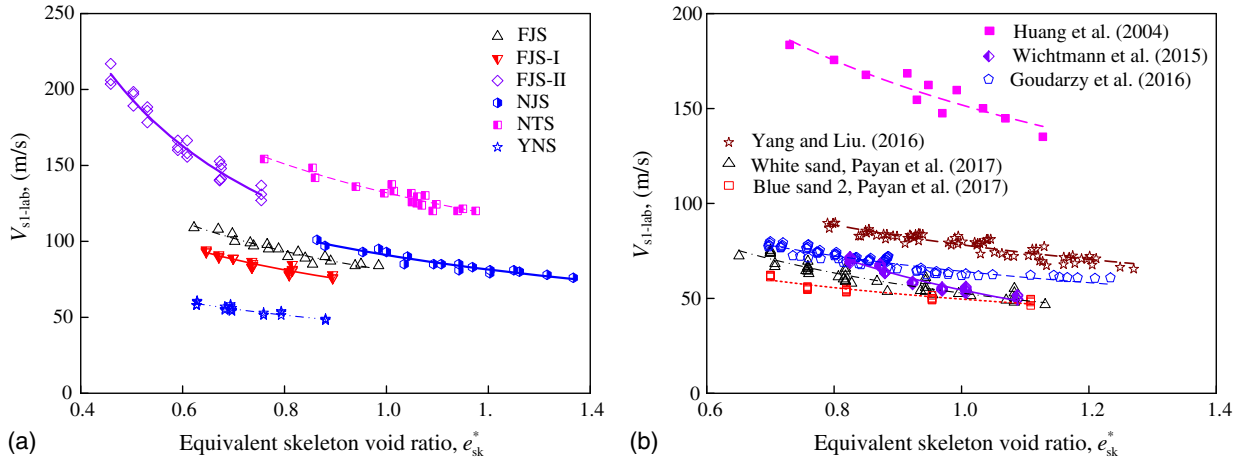

Fig. 12. Relationships between $V_{s1\text{-lab}}$ and e^*_{sk} for (a) six sandy soils in this study; and (b) six sandy soils using compiled data from the RC or BE tests of Huang et al. (2004), Wichtmann et al (2015), Goudarzy et al. (2016), Yang and Liu (2016), and Payan et al. (2017).

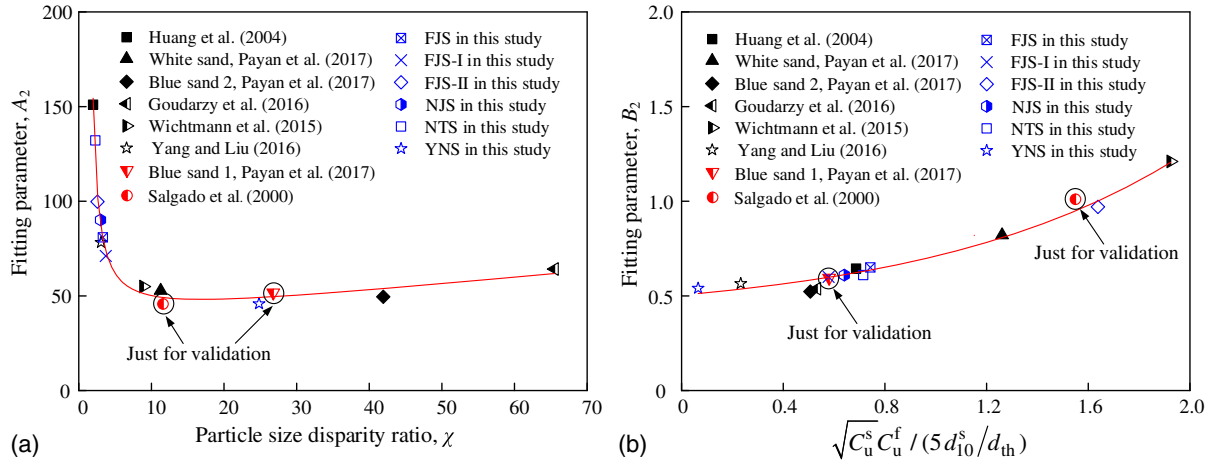

Fig. 13. Relationships between the parameters A_2, B_2 and the binary material parameters for six sandy soils in this study and six sandy soils using compiled data from the tests of Huang et al. (2004), Wichtmann et al (2015), Goudarzy et al. (2016), Yang and Liu (2016), and Payan et al. (2017), as well as validations using compiled data from the tests of Salgado et al. (2000) and Payan et al. (2017): (a) A_2 versus χ; and (b) B_2 versus $\sqrt{C_u^s}C_u^f/(5d_{10}^s/d_{th})$.

and $V_{s1\text{-field}}$ are the confining-pressure-corrected $V_{s\text{-lab}}$ and $V_{s\text{-field}}$ calculated using Eq. (7), respectively.

Fig. 12(a) presents the $V_{s1\text{-lab}}$ versus e^*_{sk} for the tested six sandy soils in this study. All of the ($V_{s1\text{-lab}}$, e^*_{sk}) data pairs of each sandy soil corresponding to the variety of d_{50}, C_u, D_r, e, e_{sk}, FC, and σ'_{c0} are located in a relatively narrow band. It is encouraging that a unique form of the relationships between $V_{s1\text{-lab}}$ and e^*_{sk} also exists for the data sets of each sandy soil. The independent test data of the measured V_s for six sandy soils in the literature (Table 2) were collected and analyzed. The compiled test data under the variety of d_{50}, C_u, D_r, e, e_{sk}, FC, and σ'_{c0} are then replotted in Fig. 12(b) in the form of $V_{s1\text{-lab}}$ versus e^*_{sk}. The best-fitting curve is shown in Fig. 12(b) and is in good agreement with the test data. Based on Fig. 12, the variation tendencies of $V_{s1\text{-lab}}$ versus e^*_{sk} follow a negative power law:

$$V_{s1\text{-lab}} = A_2(e^*_{sk})^{-B_2} \tag{8}$$

where parameters A_2 and B_2 are assumed to be material-dependent best-fitting constants.

Using generalized nonlinear regression for the experimental data of 12 sandy soils, the parameters A_2 and B_2 are closely related to the binary material property parameters (Fig. 13):

$$A_2 = D_1\chi + \frac{D_2}{\chi - D_3} + D_4 \tag{9}$$

$$B_2 = D_5 \exp\left(\frac{\sqrt{C_u^s}C_u^f}{5d_{10}^s/d_{th}}\right) + D_6 \tag{10}$$

where D_1, D_2, D_3, and D_4 = best-fitting coefficients for the set of (A_2, χ) data points, where $D_1 = 0.38$, $D_2 = 93.5$, $D_3 = 1.2$, and $D_4 = 35.3$; D_5 and D_6 = best-fitting coefficients for the set of [B_2, $\sqrt{C_u^s}C_u^f/(5d_{10}^s/d_{th})$] data points, where $D_5 = 0.12$ and $D_6 = 0.38$; correspondingly, the R-square value of a nonlinear regression for Eqs. (9) and (10) is 0.97 and 0.98, respectively. Being analogous to the discussion on the CRR prediction equation, the coefficients D_1–D_6 can be assumed to be constant independent of the type of sandy soil.

Therefore, the existence of a unique form of relationships between $V_{s1\text{-lab}}$ and e^*_{sk} for various sandy soils is convincing, and the relationship in Eq. (8) can be used to capture in a simple way the characteristics of shear-wave velocity for a wide range of sandy soils when FC is less than FC_{th}.

New Procedure for Evaluating Liquefaction Triggering

The CSR obtained from undrained CTX tests needs to be multiplied by a correction factor that considers the differences in the shearing modes and stress conditions in CTX test conditions from those of in situ soil stratum subjected to upward propagating shear waves (Seed and Peacock 1971; Chen et al. 2018). To estimate $\text{CRR}_{7.5}$ corresponding to the field CRR for an M_w 7.5 earthquake from the cyclic laboratory testing CRR_{15}, denoted as $(\text{CRR}_{15})_{\text{CTX}}$, the following equation was suggested by Seed (1979):

$$\text{CRR}_{7.5} = 0.9C_r(\text{CRR}_{15})_{\text{CTX}} \tag{11}$$

where the coefficient 0.9 accounts for the 10% reduction due to multidirectional shaking in the field (Seed and Peacock 1971). Seed (1979) suggested that the correction factor C_r was about 0.63 for normally consolidated sand deposits. However, Boulanger et al. (1998) recommended using $C_r = 0.7$ for fine-grained soils. Recent experimental data suggest that C_r may vary with soil types within the range of 0.7–0.8 for fine-grained soils (Bray and Sancio 2006; Baxter et al. 2008). Note also that there is no consensus related to C_r value (NASEM 2016). Therefore, $C_r = 0.7$ is adopted in this study.

Because the BE tests were performed under isotropic stress conditions, the V_{s1} measured in the specimen needs to be modified to an anisotropic stress condition to allow comparisons with the $V_{s1\text{-field}}$. The following equation (Baxter et al. 2008) is used here:

$$V_{s1\text{-field}} = V_{s\text{-lab}}K_0^m(P_a/\sigma'_{c0})^{2m} = V_{s1\text{-lab}}K_0^m \tag{12}$$

where K_0 = lateral earth pressure coefficient at rest, with typical values ranging between 0.4 and 0.55; and m = empirically-determined stress exponent with a value of about 0.125. The value of K_0 is assumed to be approximately 0.5 at natural, level ground sites where liquefaction has occurred or is likely to occur (Andrus and Stokoe 2000). $K_0 = 0.5$ is adopted in this study.

The predicted $\text{CRR}_{7.5}$ versus $V_{s1\text{-field}}$ correlations for six sandy soils tested in this study and the data compiled from the results of Huang et al. (2004) for one other sandy soil are plotted in Fig. 14. For comparison, the compiled field liquefaction triggering curves developed by Andrus and Stokoe (2000), Kayen et al. (2013), and Chen et al. (2017), referred to as *field curves*, are included in Fig. 14. As shown in Fig. 14, a $\text{CRR}_{7.5}$ versus $V_{s1\text{-field}}$ relationship from laboratory data is expected to be soil-specific and not unique for natural sandy soils; these soil-specific boundary curves shift to the left of the field curves. The position of a laboratory-based $\text{CRR}_{7.5}$ versus $V_{s1\text{-field}}$ curve relative to the field curves is affected by many factors, e.g., liquefaction criterion, method for measuring V_s, and empirical correlations used to convert both $(\text{CRR}_{15})_{\text{CTX}}$ to $\text{CRR}_{7.5}$ and $V_{s1\text{-lab}}$ to $V_{s1\text{-field}}$, and so on. Despite these uncertainties, one can observe that even for appreciable changes in the index properties, both $(\text{CRR}_{15})_{\text{CTX}}$ and $V_{s1\text{-lab}}$ decreased with increasing e^*_{sk} irrespective of FC, and a nearly unique $\text{CRR}_{7.5}$ versus $V_{s1\text{-field}}$ relationship exists when $FC < FC_{th}$.

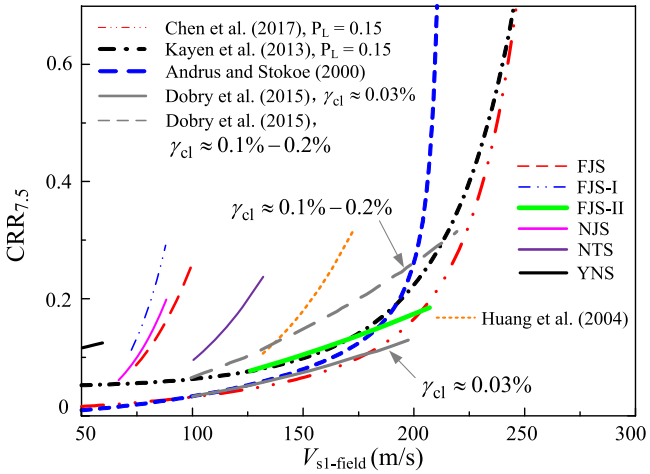

Fig. 14. Comparison of the laboratory-based $\text{CRR}_{7.5}$-$V_{s1\text{-field}}$ correlations in this paper with the curve using compiled data from the tests of Huang et al. (2004) and the V_s-based liquefaction triggering curves for earthquakes of magnitude 7.5 [revised using the Andrus and Stokoe (2000), and Kayen et al. (2013), Dobry et al. (2015), and Chen et al. (2017) curves].

Further Discussion

To facilitate the use of the proposed liquefaction triggering evaluation procedure in practice, a framework for evaluating seismic liquefaction potential is presented in Fig. 15. For a sandy soil in a real site profile, a soil-specific liquefaction triggering curve of $\text{CRR}_{7.5}$ versus $V_{s1\text{-field}}$ using the index properties can be plotted. Subsequently, at a given depth of the real soil profile, the $\text{CSR}_{7.5}$ as an equivalent value of CSR for an M_w 7.5 earthquake, which is a measure of seismic demand on a soil element for liquefaction triggering assessment, can be calculated by, for example, the Boulanger and Idriss (2012) method, then a data pair ($\text{CSR}_{7.5}$, $V_{s1\text{-field}}$) can be determined. Soil liquefaction is said to occur if $\text{CSR}_{7.5} > \text{CRR}_{7.5}$; otherwise, no soil liquefaction occurs.

The proposed procedure and the conventional procedures based on cyclic laboratory testing and/or in situ testing (SPT, CPT, and V_s testing) are different. By introducing an intrinsic physical proxy e^*_{sk}, the empirical correlations between CRR_{15} and e^*_{sk} [Eq. (4) combined with Eqs. (5) and (6)] and between V_{s1} and e^*_{sk} [Eq. (8) combined with Eqs. (9) and (10)] offer a significant advantage over other methods of estimating CRR_{15} and V_{s1} in the determination of soil-specific parameters defining the relationships. Note that PSD, e, $e_{\min}$, and $e_{\max}$ are basic properties of a soil that can be determined using routine tests. Compared with cyclic laboratory tests and in situ tests, index property tests are simple, rapid, and more economical with less uncertainty.

As seen in Figs. 11, 13, and 16, the proposed correlations for Eq. (4) [combined with Eqs. (5) and (6)] and for Eq. (8) [combined with Eqs. (9) and (10)] are validated by the independent experimental data of Xenaki and Athanasopoulos (2003), Hsiao et al. (2015), and Akhila et al. (2019) and the data of Salgado et al. (2000) and Payan et al. (2017), respectively. Tables 5 and 6 present the index properties and basic test information of five sandy soils for independent validation. It is observed that the proposed Eqs. (5), (6), (9), and (10) can be successfully applied to determine the parameters A_1, B_1, A_2, and B_2 using the basic index properties for the various sandy soils. Fig. 16 exemplifies that the proposed Eqs. (4) and (8) can be successfully applied to evaluate CRR_{15} and V_{s1} for a sandy soil, respectively.

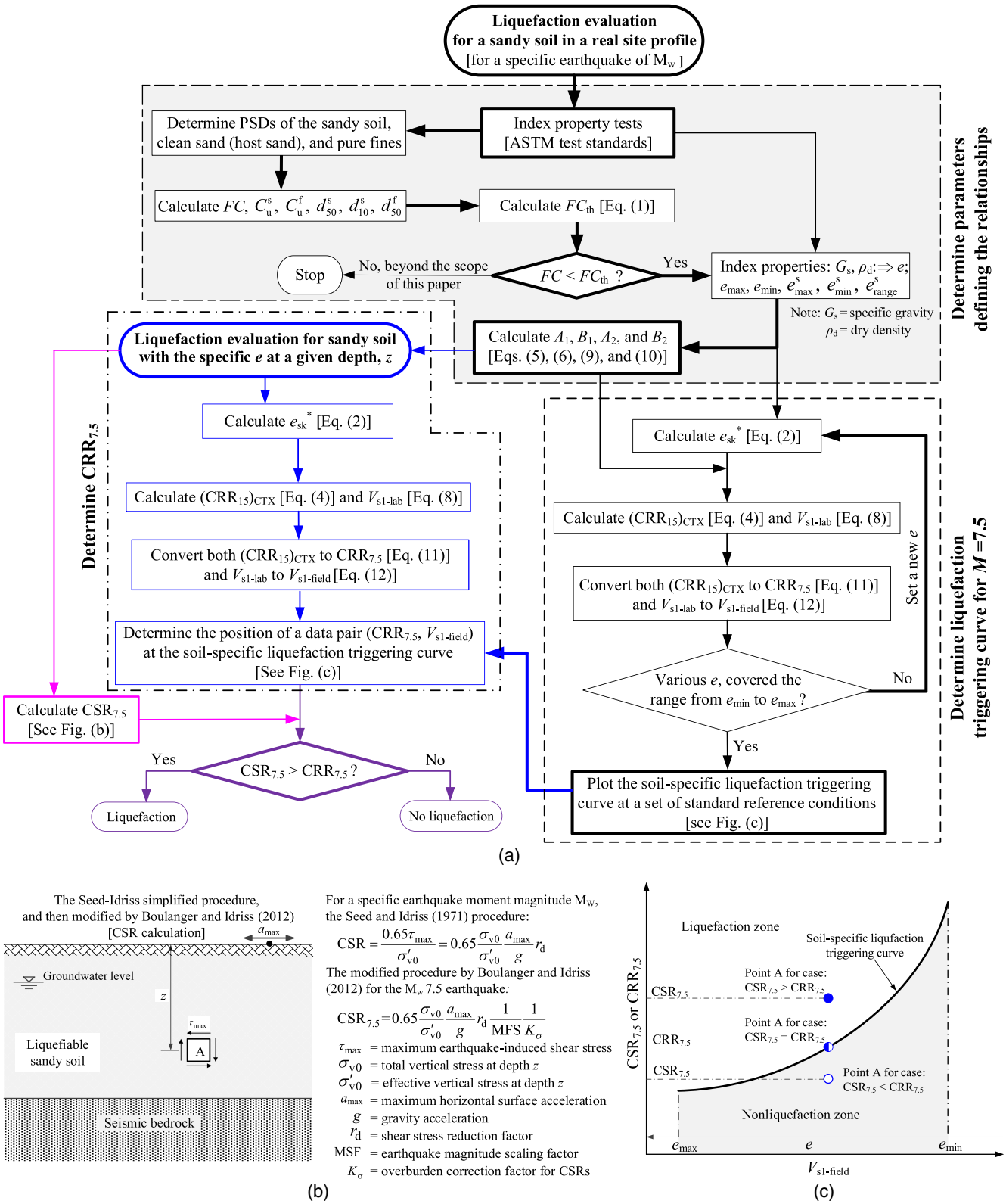

Fig. 15. A framework for evaluating sandy soil liquefaction potential during earthquakes using the proposed procedure in this study: (a) flow chart for evaluating sandy soil liquefaction potential; (b) seismic demand (CSR) analysis on a soil element within the soil profile; and (c) relationship between the liquefaction potential on a soil element at a given depth and the liquefaction triggering curve of a sandy soil in a site profile.

Fig. 14 shows two lower bounds of liquefaction occurrence corresponding to the cyclic shear strain amplitude $\gamma_{cl} \approx 0.03\%$ and $\gamma_{cl} \approx 0.1\%$–$0.2\%$ (Dobry et al. 2015). The limiting value of γ_{cl} in the field ranges from $\gamma_{cl} \approx 0.03\%$–$0.3\%$ or at most 0.6% for an M_w7.5 earthquake, and the corresponding curve of $\gamma_{cl} \approx 0.03\%$ is the lower boundary of field curves (Dobry and Abdoun 2015). In comparison, the limiting values of γ_{cl} below which there are no liquefaction case histories computed by Rodriguez-Arriaga

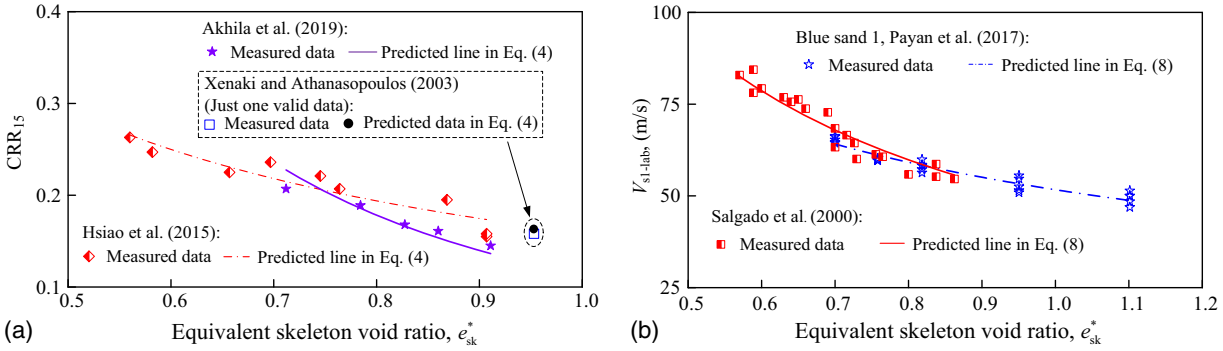

Fig. 16. Independent validations: (a) relationships between CRR_{15} and e^*_{sk} using compiled data from the undrained CTX tests of Xenaki and Athanasopoulos (2003), Hsiao et al. (2015), and Akhila et al. (2019); and (b) relationships between $V_{s1\text{-lab}}$ and e^*_{sk} using compiled data from the BE tests of Salgado et al. (2000) and the RC tests of Payan et al. (2017).

and Green (2018) for the Kayen et al. (2013) V_s database is 0.03% and for the Boulanger and Idriss (2012) SPT database is 0.05%, which are quite consistent with the limiting value γ_{cl} of Dobry and Abdoun (2015) for the lower boundary of liquefaction cases. A more rational interpretation for the liquefaction case histories is that when $\gamma_{cl} > 0.5\%$, liquefaction is very likely, and when $\gamma_{cl} < 0.03\%$, liquefaction is very unlikely. However, the γ_{cl} in undrained stress-controlled CTX tests is defined as the double-amplitude cyclic shear strain in the last cycle before reaching $r_u = 1.0$ for the first time. The values of ε_{da} during most of the test remained much smaller than 1%, increasing rapidly only in the last few cycles up to 1.3%–6.6% before initial liquefaction (Fig. 3). These undrained cyclic axial strains should be multiplied by 1.5 to obtain the shear strains. Thus, in this experimental investigation $\gamma_{cl} \geq 2\%$ or even as high as 10%.

It is interesting to note a significant gap between the values of γ_{cl} obtained from the cyclic laboratory tests and from the field curves. The difference is mainly due to the following three factors (Dobry and Abdoun 2015): (1) the greater shaking duration corresponding to the M_w 7.5 earthquake in the field, compared with the 10 or 15 cycles used in the laboratory tests; (2) the two-dimensional nature of horizontal ground shaking in the field compared with the one-dimensional cyclic straining for the laboratory tests; and (3) the redistribution of excess pore-water pressures from the lower to the upper of the deposit and upward water flow in the field that results in larger liquefiable soil mass in the field. Considering Factors (1) and (2), the $\gamma_{cl} \approx 0.03\%$ from the field curves may be updated as $\gamma_{cl} \approx 0.06\%$–$0.12\%$ for a duration of 10 cycles and unidirectional shaking field conditions. However, the updated values are still much smaller than that obtained in the laboratory tests. This gap is probably due to Factor (3). While a value of $r_u < 1.0$ measured in CTX tests implies that liquefaction is not triggered, the $r_u < 1.0$ can result in damage to nearby infrastructure in the field. Note that for the vast majority of the field case histories used to develop the field curves, ground failure evidence at the surface was used to infer whether liquefaction was triggered or not and r_u is unknown.

Conclusions

The present study aimed to explore whether the cyclic resistance (CRR_{15} in 15 cycles) and the corrected shear-wave velocity (V_{s1}) are uniquely related for a range of sandy soils. Based on the results from a comprehensive experimental study and a careful analysis of literature data, the main conclusions of the study can be summarized as follows:

1. Using the concept of binary packings, the threshold fines content FC_{th} for distinguishing the regime of *fines in sand* from *sand in fines* for sand-fines mixtures is shown to be an essential index that depends mainly on the physical properties of the soils.
2. When $FC < FC_{th}$, the liquefaction resistance, represented by CRR_{15}, is virtually uniquely related to the so-called equivalent skeleton void ratio e^*_{sk} for the range of sandy soils investigated. A unique form of the relationships between V_{s1} and e^*_{sk} for various sandy soils also exists. As e^*_{sk} is essentially an intrinsic physical index for a binary packing, the parameters in the relationship between CRR_{15} and e^*_{sk} [A_1 and B_1 in Eq. (4)] and in the relationship between V_{s1} and e^*_{sk} [A_2 and B_2 in Eq. (8)] can be determined using basic indices of the host sand and fines. The proposed correlations [Eqs. (4)–(6) and (8)–(10)] are independently validated using the experiment data from the literature.
3. By converting laboratory testing conditions to field conditions, a unique relationship can be established between the liquefaction resistance for an M_w 7.5 earthquake, $CRR_{7.5}$, and the corrected in situ shear-wave velocity, $V_{s1\text{-field}}$, through the state index e^*_{sk}. This leads to a promising simple, rapid, and economical method with less uncertainty for liquefaction evaluation of sandy soils which only involves intrinsic index properties of the soils.

Acknowledgments

The financial support provided by the National Key Research and Development Program of China (2018YFC1504301), the Natural Science Foundation of China (51978334), and the Research Grants Council of Hong Kong (17206418) is gratefully acknowledged.

References

Ahmadi, M. M., and N. A. Paydar. 2014. "Requirements for soil-specific correlation between shear wave velocity and liquefaction resistance of sands." *Soil Dyn. Earthquake Eng.* 57 (Feb): 152–163. https://doi.org/10.1016/j.soildyn.2013.11.001.

Akhila, M., K. Rangaswamy, and N. Sankar. 2019. "Undrained response and liquefaction resistance of sand–silt mixtures." *Geotech. Geol. Eng.* 37 (4): 2729–2745. https://doi.org/10.1007/s10706-018-00790-0.

Amini, F., and G. Z. Qi. 2000. "Liquefaction testing of stratified silty sands." *J. Geotech. Geoenviron. Eng.* 126 (3): 208–217. https://doi.org/10.1061/(ASCE)1090-0241(2000)126:3(208).

Andrus, R. D., and K. H. Stokoe II. 2000. "Liquefaction resistance of soils from shear–wave velocity." *J. Geotech. Geoenviron. Eng.* 126 (11):

1015–1025. https://doi.org/10.1061/(ASCE)1090-0241(2000)126:11(1015).
ASTM. 2011. *Standard practice for classification of soils for engineering purposes (unified soil classification system)*. ASTM D2487. West Conshohocken, PA: ASTM.
ASTM. 2013. *Standard test method for load controlled cyclic triaxial strength of soil*. ASTM D5311/D5311M. West Conshohocken, PA: ASTM.
Baxter, C. D. P., A. S. Bradshaw, R. A. Green, and J. H. Wang. 2008. "Correlation between cyclic resistance and shear-wave velocity for providence silts." *J. Geotech. Geoenviron. Eng.* 134 (1): 37–46. https://doi.org/10.1061/(ASCE)1090-0241(2008)134:1(37).
Boulanger, R. W., and I. M. Idriss. 2006. "Liquefaction susceptibility criteria for silts and clays." *J. Geotech. Geoenviron. Eng.* 132 (11): 1413–1426. https://doi.org/10.1061/(ASCE)1090-0241(2006)132:11(1413).
Boulanger, R. W., and I. M. Idriss. 2012. "Probabilistic standard penetration test-based liquefaction triggering procedure." *J. Geotech. Geoenviron. Eng.* 138 (10): 1185–1195. https://doi.org/10.1061/(ASCE)GT.1943-5606.0000700.
Boulanger, R. W., M. W. Meyers, L. H. Mejia, and I. M. Idriss. 1998. "Behavior of a fine-grained soil during the Loma Prieta earthquake." *Can. Geotech. J.* 35 (1): 146–158. https://doi.org/10.1139/t97-078.
Bray, J. D., and R. B. Sancio. 2006. "Assessment of the liquefaction susceptibility of fine-grained soils." *J. Geotech. Geoenviron. Eng.* 132 (9): 1165–1177. https://doi.org/10.1061/(ASCE)1090-0241(2006)132:9(1165).
Cetin, K. O., R. B. Seed, R. E. Kayen, R. E. S. Moss, H. T. Bilge, M. Ilgac, and K. Chowdhury. 2018. "SPT-based probabilistic and deterministic assessment of seismic soil liquefaction triggering hazard." *Soil Dyn. Earthquake Eng.* 115 (Dec): 698–709. https://doi.org/10.1016/j.soildyn.2018.09.012.
Cetin, K. O., R. B. Seed, A. D. Kiureghian, K. Tokimatsu, L. F. Harder, R. E. Kayen, and R. E. S. Moss. 2004. "Standard penetration test-based probabilistic and deterministic assessment of seismic soil liquefaction potential." *J. Geotech. Geoenviron. Eng.* 130 (12): 1314–1340. https://doi.org/10.1061/(ASCE)1090-0241(2004)130:12(1314).
Chang, W. J., and M. L. Hong. 2008. "Effects of clay content on liquefaction characteristics of gap-graded clayey sands." *Soils Found.* 48 (1): 101–114. https://doi.org/10.3208/sandf.48.101.
Chen, G. X., M. Y. Kong, K. Sara, W. Y. Chen, and X. J. Li. 2017. "Calibration of V_s-based empirical models for assessing soil liquefaction potential using expanded database." *Bull. Eng. Geol. Environ.* 78 (2): 1–13. https://doi.org/10.1007/s10064-017-1146-9.
Chen, G. X., Q. Wu, T. Sun, K. Zhao, E. Q. Zhou, L. Y. Xu, and Y. G. Zhou. 2018. "Cyclic behaviors of saturated sand gravel mixtures under undrained cyclic triaxial loading." *J. Earthquake Eng.*. https://doi.org/10.1080/13632469.2018.1540370.
Chen, G. X., Q. Wu, Z. L. Zhou, W. J. Ma, W. Y. Chen, K. Sara, and J. Yang. 2020. "Undrained anisotropy and cyclic resistance of saturated silt subjected to various patterns of principal stress rotation." *Géotechnique.* 70 (4): 317–331. https://doi.org/10.1680/jgeot.18.P.180.
Chen, G. X., L. Y. Xu, M. Y. Kong, and X. J. Li. 2015. "Calibration of a CRR model based on an expanded SPT-based database for assessing soil liquefaction potential." *Eng. Geol.* 196 (Sep): 305–312. https://doi.org/10.1016/j.enggeo.2015.08.002.
Chen, G. X., D. F. Zhao, W. Y. Chen, and C. H. Juang. 2019. "Excess pore water pressure generation in cyclic undrained testing." *J. Geotech. Geoenviron. Eng.* 145 (7): 04019022. https://doi.org/10.1061/(ASCE)GT.1943-5606.0002057.
Chen, G. X., Z. L. Zhou, H. Pan, T. Sun, and X. J. Li. 2016. "The influence of undrained cyclic loading patterns and consolidation states on the deformation features of saturated fine sand over a wide strain range." *Eng. Geol.* 204 (Apr): 77–93. https://doi.org/10.1016/j.enggeo.2016.02.008.
Dash, H. K., T. G. Sitharam, and B. A. Baudet. 2010. "Influence of non-plastic fines on the response of a silty sand to cyclic loading." *Soils Found.* 50 (5): 695–704. https://doi.org/10.3208/sandf.50.695.
Dobry, R., and T. Abdoun. 2015. "Cyclic shear strain needed for liquefaction triggering and assessment of overburden pressure factor K_σ." *J. Geotech. Geoenviron. Eng.* 141 (11): 04015047. https://doi.org/10.1061/(ASCE)GT.1943-5606.0001342.
Dobry, R., T. Abdoun, K. H. Stokoe II, R. E. S. Moss, M. Hatton, and H. El Ganainy. 2015. "Liquefaction potential of recent fills versus natural sands located in high-seismicity regions using shear-wave velocity." *J. Geotech. Geoenviron. Eng.* 141 (3): 04014112. https://doi.org/10.1061/(ASCE)GT.1943-5606.0001239.
Dobry, R., R. S. Ladd, F. Y. Yokel, R. M. Chung, and D. Powell. 1982. *Prediction of pore water pressure buildup and liquefaction of sands during earthquakes by the cyclic strain method: NBS Building Science Series 138*. Gaithersburg, MD: National Bureau of Standards.
Evans, M. D., and S. P. Zhou. 1995. "Liquefaction behavior of sand-gravel composites." *J. Geotech. Eng.* 121 (3): 287–298. https://doi.org/10.1061/(ASCE)0733-9410(1995)121:3(287).
Goudarzy, M., M. M. Rahman, D. Konig, and T. Schanz. 2016. "Influence of non-plastic fines content on maximum shear modulus of granular materials." *Soils Found.* 56 (6): 973–983. https://doi.org/10.1016/j.sandf.2016.11.003.
Green, R. A., and G. A. Terri. 2005. "Number of equivalent cycles concept for liquefaction evaluations—Revisited." *J. Geotech. Geoenviron. Eng.* 131 (4): 477–488. https://doi.org/10.1061/(ASCE)1090-0241(2005)131:4(477).
Hsiao, D. H., V. T. A. Phan, Y. T. Hsieh, and H. Y. Kuo. 2015. "Engineering behavior and correlated parameters from obtained results of sand–silt mixtures." *Soil Dyn. Earthquake Eng.* 77 (Oct): 137–151. https://doi.org/10.1016/j.soildyn.2015.05.005.
Huang, Y. T., A. B. Huang, Y. C. Kuo, and M. D. Tsai. 2004. "A laboratory study on the undrained strength of a silty sand from Central Western Taiwan." *Soil Dyn. Earthquake Eng.* 24 (9–10): 733–743. https://doi.org/10.1016/j.soildyn.2004.06.013.
Idriss, I. M., and R. W. Boulanger. 2010. *SPT-based liquefaction triggering procedures*. Report UCD/CGM-10/02. Davis, CA: Center for Geotechnical Modeling, Univ. of California, Davis.
Kayen, R., R. E. S. Moss, E. M. Thompson, R. B. Seed, K. O. Cetin, A. D. Kiureghian, Y. Tanaka, and K. Tokimatsu. 2013. "Shear-wave velocity-based probabilistic and deterministic assessment of seismic soil liquefaction potential." *J. Geotech. Geoenviron. Eng.* 139 (3): 407–419. https://doi.org/10.1061/(ASCE)GT.1943-5606.0000743.
Kim, U., D. Kim, and L. Zhuang. 2016. "Influence of fines content on the undrained cyclic shear strength of sand-clay mixtures." *Soil Dyn. Earthquake Eng.* 83 (Apr): 124–134. https://doi.org/10.1016/j.soildyn.2016.01.015.
Ku, C. S., C. H. Juang, C. W. Chang, and J. Ching. 2012. "Probabilistic version of the Robertson and Wride method for liquefaction evaluation: Development and application." *Can. Geotech. J.* 49 (1): 27–44. https://doi.org/10.1139/t11-085.
Kuerbis, R. H. 1989. "The effect of gradation and fines content on the undrained loading response of sand." B.A.Sc. thesis, Dept. of Civil Engineering, Univ. of British Columbia.
Lade, P. V., and J. A. Yamamuro. 1997. "Effects of nonplastic fines on static liquefaction of sands." *Can. Geotech. J.* 34 (6): 918–928. https://doi.org/10.1139/t97-052.
Martin, G. R., W. D. L. Finn, and H. B. Seed. 1975. "Fundamentals of liquefaction under cyclic loading." *J. Geotech. Eng. Div.* 101 (GT5): 423–438. https://doi.org/10.1016/0148-9062(75)92420-1.
Mohammadi, A., and A. Qadimi. 2015. "A simple critical state approach to predicting the cyclic and monotonic response of sands with different fines contents using the equivalent intergranular void ratio." *Acta Geotech.* 10 (5): 587–606. https://doi.org/10.1007/s11440-014-0318-z.
Moss, R. E. S., R. B. Seed, R. E. Kayen, J. P. Stewart, A. Der Kiureghian, and K. O. Cetin. 2006. "CPT-based probabilistic and deterministic assessment of in situ seismic soil liquefaction potential." *J. Geotech. Geoenviron. Eng.* 132 (8): 1032–1051. https://doi.org/10.1061/(ASCE)1090-0241(2006)132:8(1032).
NASEM (National Academies of Sciences, Engineering, and Medicine). 2016. *State of the art and practice in the assessment of earthquake-induced soil liquefaction and its consequences*. Washington, DC: National Academies Press.
Papadopoulou, A., and T. Tika. 2008. "The effect of fines on critical state and liquefaction resistance characteristics of non-plastic silty sands." *Soils Found.* 48 (5): 713–725. https://doi.org/10.3208/sandf.48.713.

Payan, M., K. Senetakis, A. Khoshghalb, and N. Khalili. 2017. "Characterization of the small-strain dynamic behaviour of silty sands; contribution of silica non-plastic fines content." *Soil Dyn. Earthquake Eng.* 102 (Nov): 232–240. https://doi.org/10.1016/j.soildyn.2017.08.008.

Polito, C. P., and J. R. Martin II. 2001. "Effects of nonplastic fines on the liquefaction resistance of sands." *J. Geotech. Geoenviron. Eng.* 127 (5): 408–415. https://doi.org/10.1061/(ASCE)1090-0241(2001)127:5(408).

Rahman, M. M., and S. R. Lo. 2008. "The prediction of equivalent granular steady state line of loose sand with fines." *Geomech. Geoeng. Int. J.* 3 (3): 179–190. https://doi.org/10.1080/17486020802206867.

Rahman, M. M., S. R. Lo, and M. A. L. Baki. 2011. "Equivalent granular state parameter and undrained behaviour of sand–fines mixtures." *Acta Geotech.* 6 (4): 183–194. https://doi.org/10.1007/s11440-011-0145-4.

Rahman, M. M., S. R. Lo, and C. T. Gnanendran. 2009. "Reply to the discussion by Wanatowski and Chu on 'On equivalent granular void ratio and steady state behaviour of loose sand with fines.'" *Can. Geotech. J.* 46 (4): 483–486. https://doi.org/10.1139/T09-025.

Robertson, P. K. 2009. "Interpretation of cone penetration tests–A unified approach." *Can. Geotech. J.* 46 (11): 1337–1355. https://doi.org/10.1139/T09-065.

Robertson, P. K., and C. E. Wride. 1998. "Evaluating cyclic liquefaction potential using the cone penetration test." *Can. Geotech. J.* 35 (3): 442–459. https://doi.org/10.1139/t98-017.

Rodriguez-Arriaga, E., and R. A. Green. 2018. "Assessment of the cyclic strain approach for evaluating liquefaction triggering." *Soil Dyn. Earthquake Eng.* 113 (Oct): 202–214. https://doi.org/10.1016/j.soildyn.2018.05.033.

Salgado, R., P. Bandini, and A. Karim. 2000. "Shear strength and stiffness of silty sand." *J. Geotech. Geoenviron. Eng.* 126 (5): 451–462. https://doi.org/10.1061/(ASCE)1090-0241(2000)126:5(451).

Seed, H. B. 1979. "Soil liquefaction and cyclic mobility evaluation for level ground during earthquakes." *J. Geotech. Eng. Div.* 105 (2): 201–255. https://doi.org/10.1016/0148-9062(79)91243-9.

Seed, H. B., and I. M. Idriss. 1971. "Simplified procedure for evaluating soil liquefaction potential." *J. Soil Mech. Found. Div.* 97 (SM9): 1249–1273.

Seed, H. B., and W. H. Peacock. 1971. "Test procedures for measuring soil liquefaction characteristics." *J. Soil Mech. Found. Div.* 97 (SM8): 1099–1199.

Seed, H. B., K. Tokimatsu, L. F. Harder, and R. M. Chung. 1985. "Influence of SPT procedures in soil liquefaction resistance evaluations." *J. Geotech. Eng.* 111 (12): 1425–1445. https://doi.org/10.1061/(ASCE)0733-9410(1985)111:12(1425).

Seed, R. B., et al. 2003. *Recent advances in soil engineering: A unified and consistent framework*. Earthquake Engineering Research Center Rep. No. EERC 2003-06. Berkeley, CA: Pacific Earthquake Engineering Research.

Silver, M. L., and H. B. Seed. 1971. "Deformation characteristics of sands under cyclic loading." *J. Soil Mech. Found. Div.* 97 (8): 1081–1098.

Sitharam, T. G., H. K. Dash, and R. S. Jakka. 2013. "Postliquefaction undrained shear behavior of sand-silt mixtures at constant void ratio." *Int. J. Geomech.* 13 (4): 421–429. https://doi.org/10.1061/(ASCE)GM.1943-5622.0000225.

Stamatopoulos, C. A. 2010. "An experimental study of the liquefaction strength of silty sands in terms of the state parameter." *Soil Dyn. Earthquake Eng.* 30 (8): 662–678. https://doi.org/10.1016/j.soildyn.2010.02.008.

Thevanayagam, S. 2000. "Liquefaction potential and undrained fragility of silty sands." In *Proc., 12th World Conf. Earthquake Engineering CD-ROM*. Wellington, New Zealand: New Zealand Society for Earthquake Engineering.

Thevanayagam, S., T. Shenthan, S. Mohan, and J. Liang. 2002. "Undrained fragility of clean sands, silty sands, and sandy silts." *J. Geotech. Geoenviron. Eng.* 128 (10): 849–859. https://doi.org/10.1061/(ASCE)1090-0241(2002)128:10(849).

Tokimatsu, K., T. Yamazako, and Y. Yoshimi. 1986. "Soil liquefaction evaluations by elastic shear moduli." *Soils Found.* 26 (1): 25–35. https://doi.org/10.3208/sandf1972.26.25.

Wang, J. H., K. Moran, and C. D. P. Baxter. 2006. "Correlation between cyclic resistance ratios of intact and reconstituted offshore saturated sands and silts with the same shear wave velocity." *J. Geotech. Geoenviron. Eng.* 132 (12): 1574–1580. https://doi.org/10.1061/(ASCE)1090-0241(2006)132:12(1574).

Wichtmann, T., M. A. Navarrete Hernández, and T. Triantafyllidis. 2015. "On the influence of a non-cohesive fines content on small strain stiffness, modulus degradation and damping of quartz sand." *Soil Dyn. Earthquake Eng.* 69 (Feb): 103–114. https://doi.org/10.1016/j.soildyn.2014.10.017.

Xenaki, V. C., and G. A. Athanasopoulos. 2003. "Liquefaction resistance of sand–silt mixtures: An experimental investigation of the effect of fines." *Soil Dyn. Earthquake Eng.* 23 (3): 1–12. https://doi.org/10.1016/S0267-7261(02)00210-5.

Xie, J. F. 1984. "Some comments on the formula for estimating the liquefaction of sand in revised seismic design code." [In Chinese.] *Earthquake Eng. Eng. Vib.* 4 (2): 95–126.

Yang, J., and X. Q. Gu. 2013. "Shear stiffness of granular material at small-strain: Does it depend on grain size?" *Géotechnique* 63 (2): 165–179. https://doi.org/10.1680/geot.11.P.083.

Yang, J., and X. Liu. 2016. "Shear wave velocity and stiffness of sand: The role of non-plastic fines." *Géotechnique* 66 (6): 500–514. https://doi.org/10.1680/jgeot.15.P.205.

Yang, J., S. Savidis, and M. Roemer. 2004. "Evaluating liquefaction strength of partially saturated sand." *J. Geotech. Geoenviron. Eng.* 130 (9): 975–979. https://doi.org/10.1061/(ASCE)1090-0241(2004)130:9(975).

Yang, J., and H. Y. Sze. 2011a. "Cyclic behaviour and resistance of saturated sand under non-symmetrical loading conditions." *Géotechnique* 61 (1): 59–73. https://doi.org/10.1680/geot.9.P.019.

Yang, J., and H. Y. Sze. 2011b. "Cyclic strength of sand under sustained shear stress." *J. Geotech. Geoenviron. Eng.* 137 (12): 1275–1285. https://doi.org/10.1061/(ASCE)GT.1943-5606.0000541.

Yang, J., L. M. Wei, and B. B. Dai. 2015. "State variables for silty sands: Global void ratio or skeleton void ratio?" *Soils Found.* 55 (1): 99–111. https://doi.org/10.1016/j.sandf.2014.12.008.

Youd, T. L., et al. 2001. "Liquefaction resistance of soils: Summary report from the 1996 NCEER and 1998 NCEER/NSF workshops on evaluation of liquefaction resistance of soils." *J. Geotech. Geoenviron. Eng.* 127 (10): 817–833. https://doi.org/10.1061/(ASCE)1090-0241(2001)127:10(817).

Zhuang, H. Y., R. Wang, G. X. Chen, Y. Miao, and K. Zhao. 2018. "Shear modulus reduction of saturated sand under large liquefaction-induced deformation in cyclic torsional shear tests." *Eng. Geol.* 240 (Jun): 110–122. https://doi.org/10.1016/j.enggeo.2018.04.018.